Title
CINEMATIC STUDIES OF THE ANODIC DISSOLUTION OF METALS AT HIGH CURRENT DENSITIES

Author
Hellyar, Kenneth George.

Publication Date
1971-09-01

LBL-157

c.1

CINEMATIC STUDIES OF THE ANODIC DISSOLUTION OF METALS AT HIGH CURRENT DENSITIES

Kenneth George Hellyar
(M.S. Thesis)

September 1971

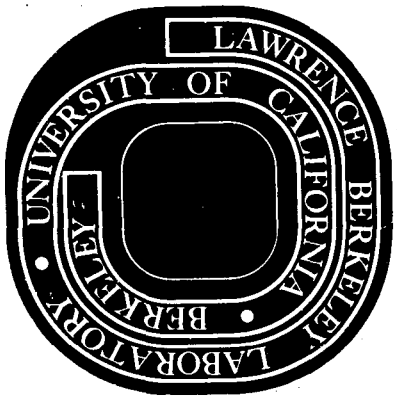

AEC Contract No. W-7405-eng-48

DISCLAIMER

Table of Contents

CINEMATIC STUDIES OF THE ANODIC DISSOLUTION OF METALS AT HIGH CURRENT DENSITIES *

Kenneth George Hellyar

Inorganic Materials Research Division, Lawrence Radiation Laboratory and Department of Chemical Engineering, University of California, Berkeley, California

ABSTRACT

Color motion picture photography combined with electrical measurements of the cell voltage (at constant current) have been used in a study of the anodic dissolution of metals at high current densities in a flowing electrolyte. Copper, nickel, carbon steel, and three nickel-based alloys were observed in 5N solutions of NaCl, $NaNO_3$, and $NaClO_3$ flowing at 10 cm/sec (Re = 750) at current densities of 1 and 20 amperes/cm^2. Some observations have also been made in free convection and forced convection up to 150 cm/sec (Re = 12,000) and current densities up to 40 amperes/cm^2. The formation of solid reaction products was observed with many metal/electrolyte combinations.

* M. S. Thesis, research conducted under the direction of R. H. Muller and C. W. Tobias.

I. INTRODUCTION

A. Electrochemical Machining

The electrochemical machining process (ECM) is fundamentally an electrolysis process occurring at high current densities (in the order of 100 amperes/cm^2 or 650 amperes/in^2) in an aqueous electrolyte. For comparison, typical electroplating current densities in an aqueous electrolyte are 10^{-2} to 10^{-1} amperes/cm^2. Electrolysis of fused salts may employ current densities in the order of 1 to 10 amperes/cm^2.

With ECM, a metal is anodically dissolved from a selected region of a metallic workpiece, at a rate governed by electrochemical laws. Extremely hard, high-temperature metals, such as those used in jet turbines, have been commercially machined by this technique and it seems likely that ECM will replace conventional machining techniques in other areas, such as the machining of gears.[1-3]

In the language of the traditional machining processes, ECM uses the workpiece as the anode and the tool as the cathode in an electrolysis reaction. By immersing the tool and the workpiece in an electrolyte and passing large currents between the two, the 'tool' can be made to electrochemically 'machine' the 'workpiece'. The tool is approximately a replica of the finished workpiece, that is, the tool and workpiece 'fit' together like a casting and its mold. As an example, tubes are used for electrochemically 'drilling' holes. In actual practice, the tool configurations required to produce even a simple finished workpiece must be found by empirical means.

Upon passing a current between the electrodes, the reactions at the anodic workpiece include the oxidation of the metal and/or electrolyte. This generally results in the dissolution of the metal

and/or oxygen evolution. The cathodic tool reactions include the reduction of the tool and/or electrolyte. Since most tools are made of metals, the reactions are plating out of metal ions from the electrolyte and/or hydrogen evolution. In commercial practice, conditions are selected that will favor the dissolution of metal at the anode and evolution of hydrogen at the cathode. Plating at the cathode is undesirable since it changes the tool shape, and hence, the final shape of the workpiece.

To minimize the ohmic resistance (IR drop) through the electrolyte, a factor in the power requirement during machining, and to minimize stray currents the gap between the anode and cathode is made as small as possible (typically 0.1 to 0.5 mm). In spite of the narrowness of the gap there is an enormous amount of heat generated by the ohmic resistance, 1-5 kilowatts/cm^2. To dissipate heat, to supply reactant ions, and to remove reaction products, (solutes, solids, and gases,) the electrolyte is pumped through the gap at high flow velocities (up to several hundred cm/sec).

If the ECM process is carried out at a constant voltage and a constant tool feed rate, the current will adjust itself to maintain an equilibrium cutting gap. The reasoning is as follows. If the gap narrows, the resistance across the gap diminishes and the dissolution rate increases. Conversely, if the gap widens, the resistance increases and the dissolution rate decreases. Several investigators have developed mathematical models based on this concept in an attempt to predict the proper operating conditons for ECM.[4,5] The early development, and much of the research since then, on the ECM technique

has been toward predicting the process variables, such as the gap width, needed to produce a given workpiece.[6-9]

Recently, researchers have begun investigating the electrochemical principles involved in this high current density process. The immediate goal for many industrial researchers has been the determination of process variables, particularly new electrolyte formulations, that will provide improved surface finishes and dimensional accuracy. Other researchers seek a fundamental understanding of high current density processes, in general, by exploring the electrochemical and transport phenomena found in ECM.

Among the fundamental investigations have been polarization studies of ECM using rotating disk electrodes at high current densities conducted by Hoare, et al., Davydov, et al., and Chin.[10-12] Boden and Brook have presented an elementary review of some of the electrochemical principles of ECM.[13] Kinoshita and Landolt, et al. have studied the stoichiometry of the anodic dissolution of copper at high current densities, as well as anode potentials, and the influence of crystallographic factors.[14-19] Landolt, Acosta, et al. observed the nature of cathodic hydrogen evolution in a small electrode gap as a function of current density and flow rate.[20]

This investigation made use of high speed cinematography to observe the anode surface during dissolution. From these observations, qualitative conclusions concerning the nature of the reaction products have been derived.

B. Scope

This study sought to answer three questions, which resulted in part from the work of Kinoshita.[14] First, what was the relationship

between the phenomena observed visually during anodic dissolution and the measured voltages at constant current? In particular, what physical events were associated with the active/transpassive voltage transition? Second, how general is the formation of solid and gaseous reaction products observed during the high current density anodic dissolution of copper, in contrast with dissolved species which normally predominate at low current densities, particularly in industrially important alloys? To what extent did the chemical nature of the dissolving metal determine the mechanism by which reaction products were removed from the surface? Third, was it possible that periodicities existed for systems other than the copper/sodium chlorate system?

To answer the above questions, it was necessary to correlate photographic observations with electrical measurements and to extend those observations to different chemical and hydrodynamic systems. After considering several different techniques, an optical system was constructed in which the observed anodic dissolution events and an image of a pen recorder cell-voltage versus time trace were superimposed upon the same frame of film (see Section II. B. Optical system). Such a superposition allowed a direct comparision of observed phenomena and measured cell voltages (at constant currents). To extend the observations to higher current densities and to forced convection, a flow system was constructed (see Section II.A. Flow system and Section II.C. Electrical system). This system permitted current densities up to 40 amperes/cm^2 and flow rates up to 150 cm/sec (Reynolds number equal to 12,000). Six metals (copper, nickel, carbon steel and three nickel-based alloys) were used in dissolution experiments in three

electrolytes (NaCl, $NaNO_3$ and $NaClO_3$) (see Section III. Materials: metals and electrolytes).

This study was intended to be essentially a qualitative survey of phenomena occurring at high current densities (1 - 40 amperes/cm^2). A descriptive summary of the observed phenomena is presented for the various metal/electrolyte systems studied (see Section IV. Results).

II. EXPERIMENTAL APPARATUS AND PROCEDURE

The experimental apparatus consisted of essentially three systems: a flow loop including the electrolysis cell, an optical system including the camera, and electrical circuits including the power supply. The apparatus is shown in Fig. 1 and depicted schematically in Fig. 2.

A. The Electrolysis Systems

1. The Flow System

One objective of this study was to photograph anodic dissolution events occurring in forced convection. To accomplish this, a flow channel was constructed, in which the direct observation of the anode during dissolution was possible.

In designing the flow channel, the lower limit for the anode surface area was restricted by the magnification and depth of field expected with the present optical arrangement (see Section II.B. Optical system) and the upper area limit was restricted by the available power supply, hence, the maximum attainable current density (see Section II.C. Electrical system). Considering these two factors, the planar anode surface was chosen to have dimensions of 5 mm by 5 mm.

After considering several designs, a system in which the cathodes were embedded in the channel walls at right angles to the anode was developed. This is shown in the isometric drawing of the electrode region of the flow channel, Fig. 3. The cathodes were fabricated from stainless steel and were connected in parallel to the power supply. Once the decision to use cathodes in the channel wall was made, the width of the channel was selected so cathodic hydrogen would not obscure the anode. The depth of the channel was determined by the

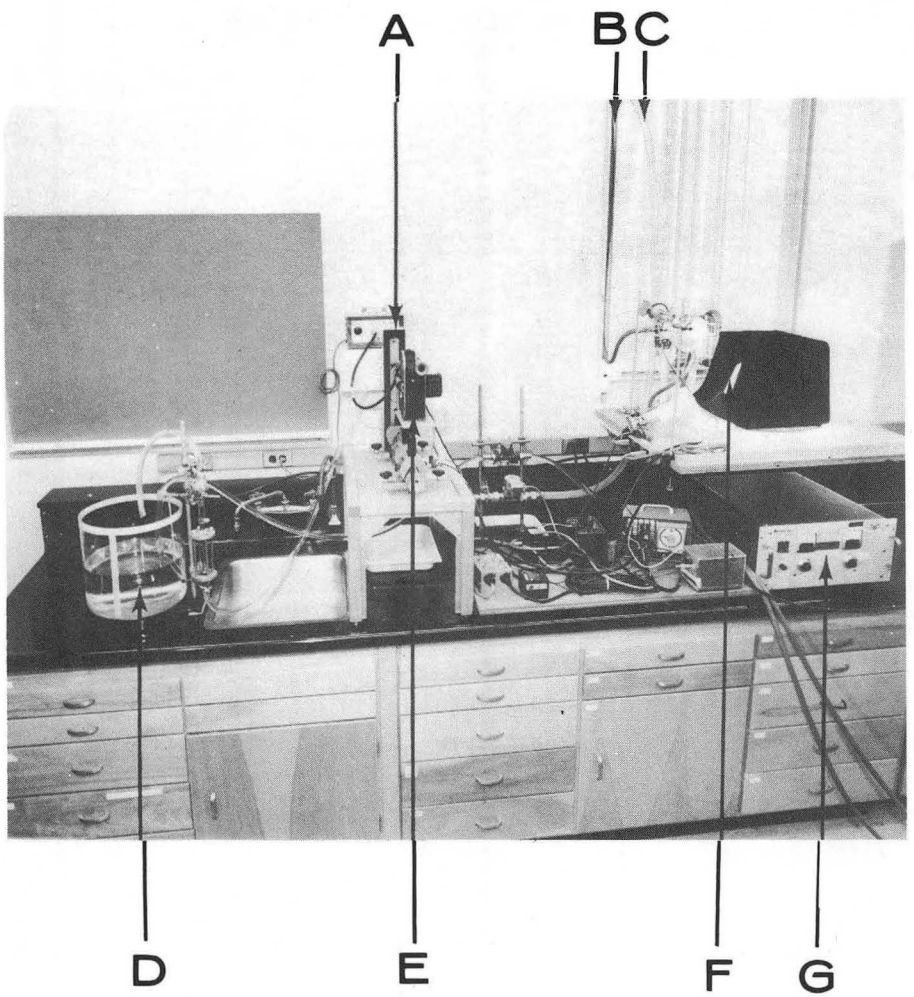

CBB 709-4266A

Fig. 1. Overall view of the experimental apparatus. A. Flow channel; the flow is from bottom to top. B. Vacuum line between aspirator and overhead tank (not shown). C. Hose from the overhead tank to the flow channel. D. Mixing tank. E. Bolex camera. F. Chart recorder (velvet mask is in place). G. Power supply.

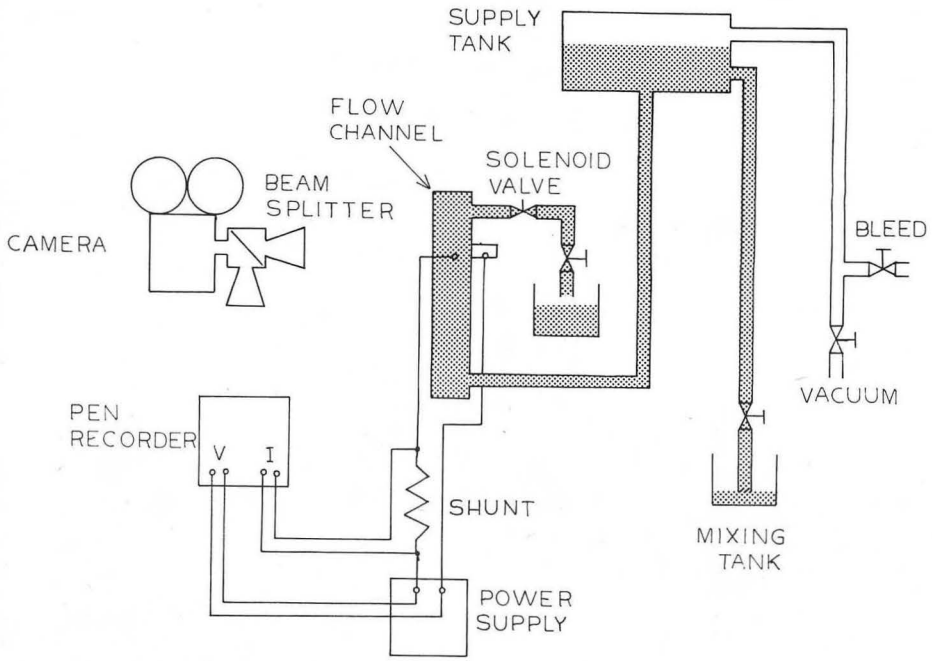

XBL 714-662

Fig. 2. Schematic diagram of the flow system.

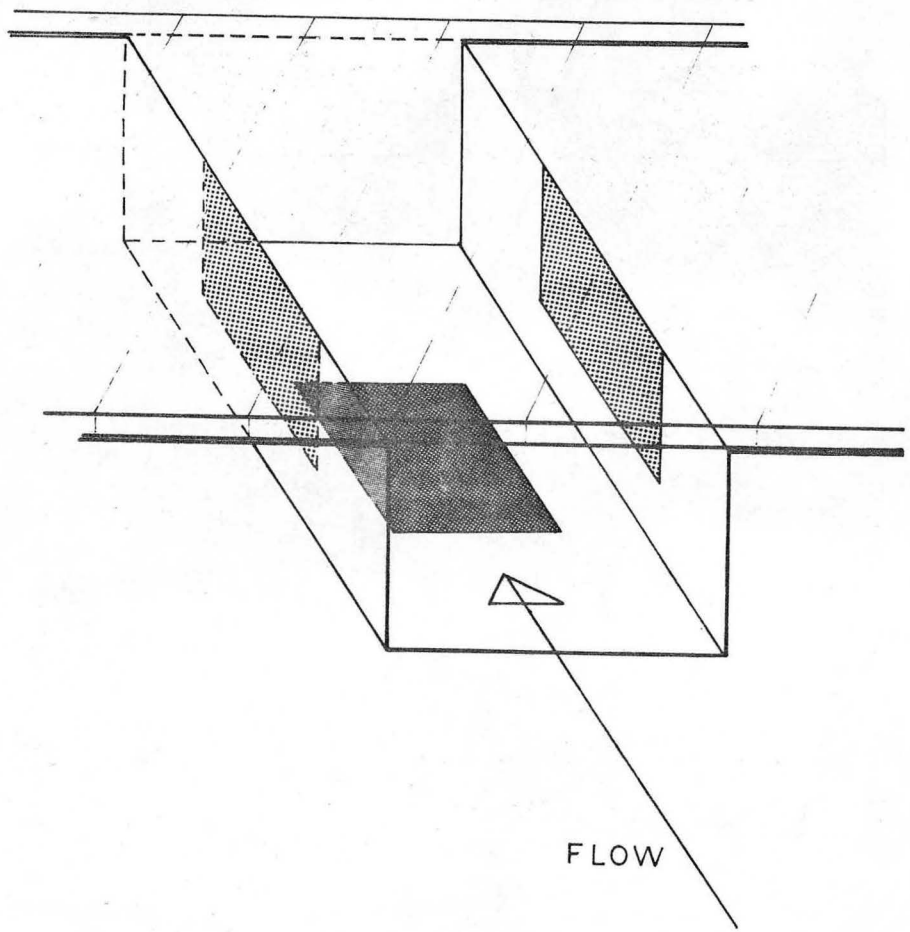

XBL 714-667

Fig. 3. A section of the flow channel in the electrode region. The anode (5 mm × 5 mm) is in the bottom of the channel. The cathodes (6.4 mm long and 4 mm deep) are embedded in the channel walls at right angles to the anode. A glass plate, through which the observations were made, forms the top of the channel. Channel cross section is 6 mm deep by 10 mm wide.

provision that the cathode area should be as large as possible and the current distribution on the anode should be as uniform as possible. (This is considered further in Section V.A. Current distribution and hydrodynamic conditions.) The resulting electrode dimensions and channel cross-section were:

anode	5 mm × 5 mm
cathode	6.4 mm long × 4 mm deep (one in each wall)
channel	10 mm wide × 6 mm deep

The electrode region of the channel is shown in Fig. 4, and in the cross-sectioned diagram, Fig. 5.

The flow channel body was machined from a single block of polypropylene with overall dimensions of 7.6 cm wide, 4.8 cm deep, and 71.0 cm long. The channel was milled as a slot in the solid polypropylene block. Electrolyte entered the channel through a fitting in the back side at the lower end of the cell body. The flow was then up the flow channel and out a similar fitting in the back side at the upper end of the flow channel. The upward flow direction was chosen so gas bubbles would be swept from the anode surface even at low flow rates. The flow exit can be seen at the end of the channel in Fig. 4. The entrance length to the electrode region was 53 cm (70 hydraulic diameters) and the downstream length was 7.6 cm (10 hydraulic diameters). The top of the channel consisted of a 1/8 inch plexiglass plate with O-ring sells between the cell body and the plate and between the plate and an aluminum retaining cover.

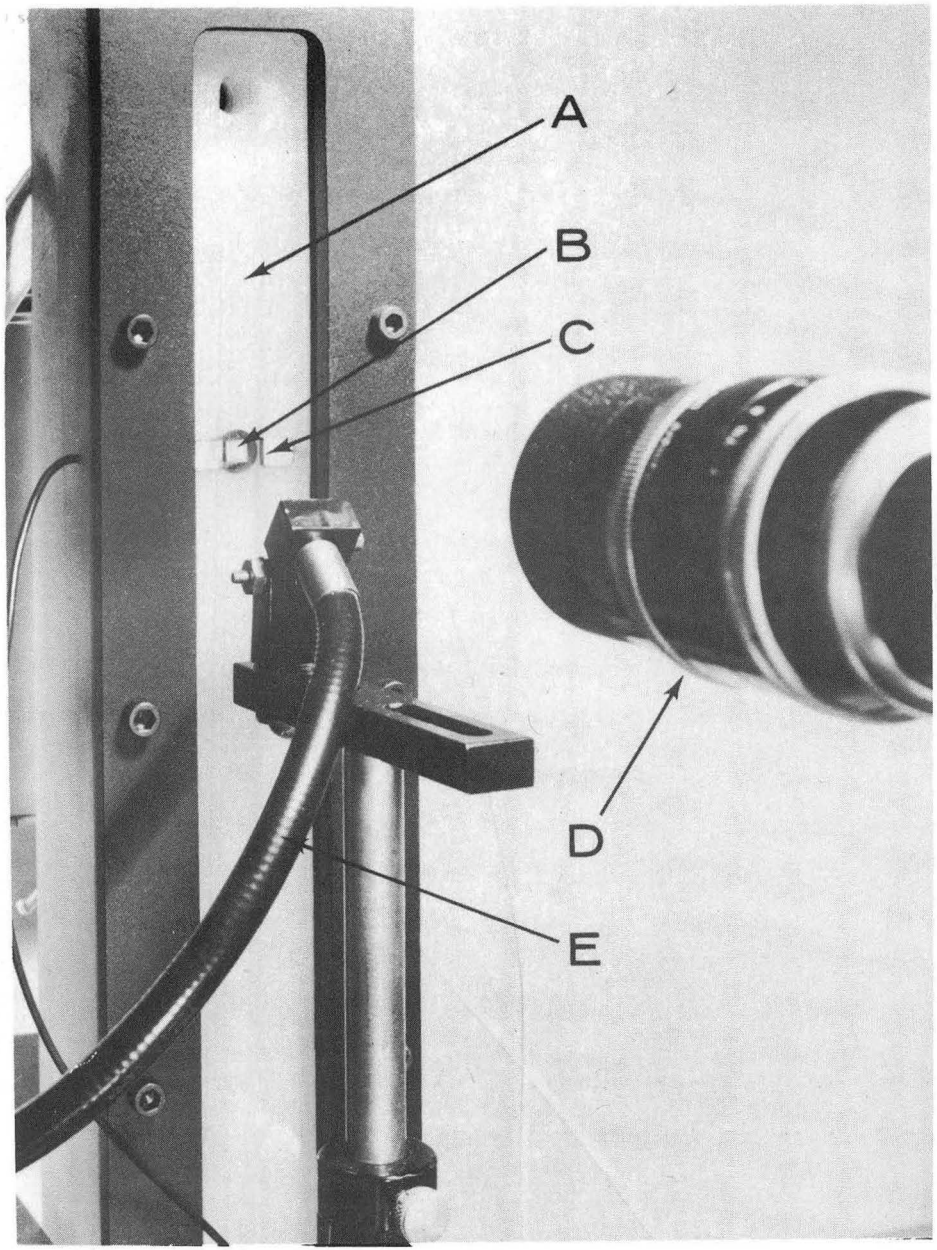

XBB 709-4268A

Fig. 4. The electrode region of the flow channel. A. Channel with electrolyte flow in the upward direction. B. The Anode surface in the bottom of the channel. C. The cathodes in the channel walls. D. Camera objective. E. Fiber optics light guide.

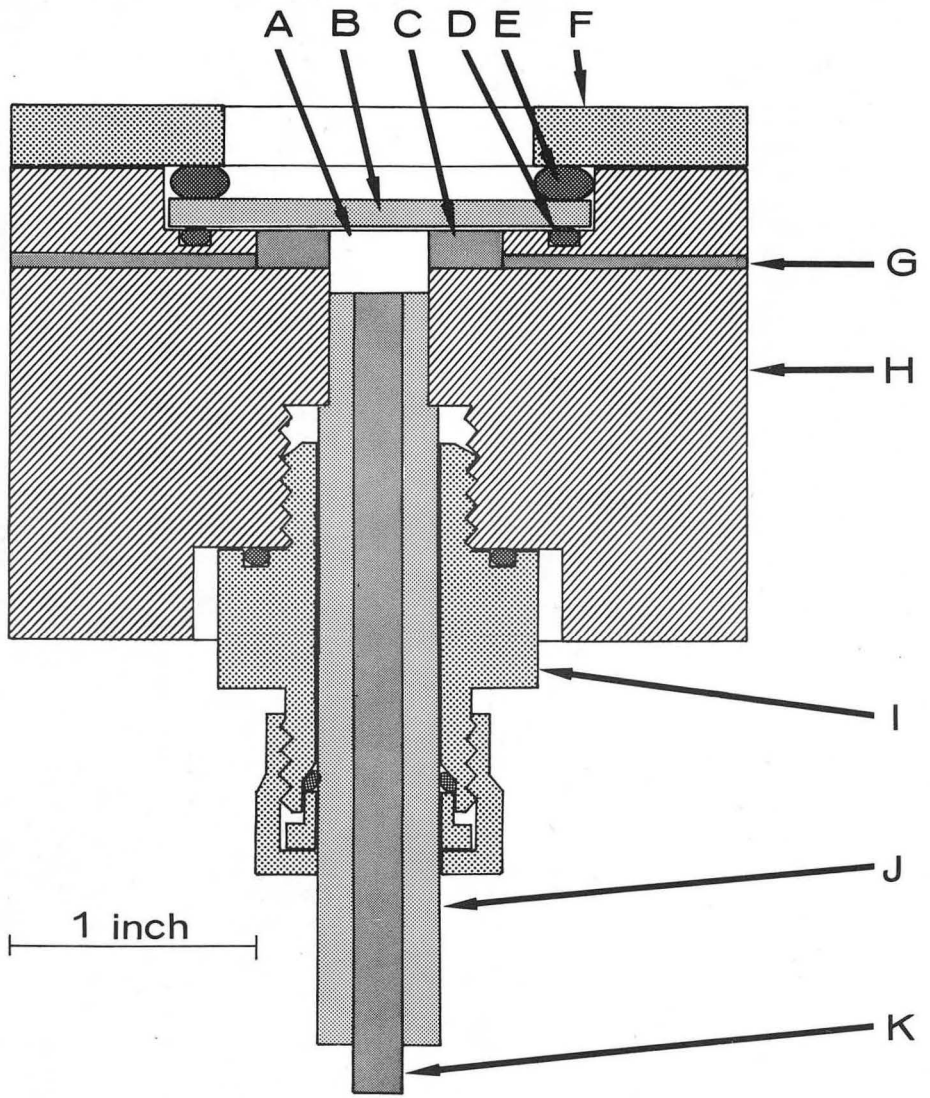

XBL 713-473

Fig. 5. Cross sectioned diagram of the flow channel in the electrode region. A. The flow channel. B. Glass plate. C. One of the two cathodes. D. and E. O-ring seals between the cell body and the glass and between the retaining cover and the glass. F. Retaining cover (bolts, not shown, hold it to the channel body). G. Electrical connection to the cathode. H. Flow channel body. I. Electrode holder. J. Epoxy covering on the anode. K. The anode.

The finished anodes were cast in epoxy and had final dimensions of approximately 8 cm long and 12 cm in diameter (see Section III. A. Metals, for details). The level of the anode surface with respect to the bottom of the flow channel was determined by a shoulder machined into the epoxy casting. The anode was held in position by an O-ring connector.* Rubber O-ring seals prevented leaking (Fig. 5).

Electrolyte flow was by gravity feed from an overhead tank. This method was selected to give a uniform flow rate at both high and low flows. The flow rate was controlled with a stainless steel needle valve. A 9 liter tank was constructed from a 60.0 cm long section of 15.2 cm diameter plexiglass pipe. The tank was mounted horizontally to minimize the change in liquid head to a maximum of 10 cm out of a total head of 3 m. During most experiments, the liquid level changed by a couple of centimeters or less. The tank had one end permanently sealed and the other end sealed with a cover and O-rings. Except for openings for applying a vacuum and for electrolyte flow in and out, the tank was air tight and could be pressurized or partially evacuated. Using only the hydraulic head, and all valves fully open, a maximum electrolyte velocity of 150 cm/sec (Re = 11,250 for water) was obtained. Most experiments were conducted at lower flow rates.

The electrolyte solution was mixed in a pyrex holding tank. By applying a vacuum to the overhead tank, the electrolyte was transferred from the mixing tank to the overhead tank. A separate line led from the overhead tank, through a solenoid valve, the flow channel, and a stainless steel needle valve to a collecting tank. The flow rate was

*Cajon Ultra-Torr Fitting 8UT-1-OR-316, Cajon Company, Solon, Ohio 44139

determined by measuring the volume of fluid collected and the duration of the electrolyte flow during each experiment. The time of flow was determined from an event marker on the pen recorder that was actuated by the solenoid valve; the valve controlled the on/off flow of the electrolyte. As an added check, the solenoid valve also actuated a time interval meter. With this arrangement, the flow rate could be measured with an accuracy of 5 percent.

For other design criteria for flow channels used for high current density studies in this laboratory, see Landolt.[17]

2. The Stagnant Cell

For selected experiments with copper, and preliminary exposure tests with various optical systems and films, a stagnant cell was constructed. This is shown in Fig. 6.

Anodes were fabricated from cold drawn OFHC copper rods (see Table 1) and insulated with varnish.* The cathode was fabricated from a $7\frac{1}{2}$ cm by $7\frac{1}{2}$ cm piece of 16 mesh stainless steel screen. A porous barrier of 6.3 mm thick nylon mesh pad in a plexiglass holder was used to prevent mixing of the anolyte and catholyte.

The anode, cathode, and barrier were placed in a rectangular tank. The tank was constructed of plexiglass with plate glass for the front and back sides. Photographs of the anode were taken through the front side. During experiments, the tank contained 1.0 liter of solution.

*G. E. Adhesive and Insulating Varnish, No. 7031, General Electric, Schenectady, New York.

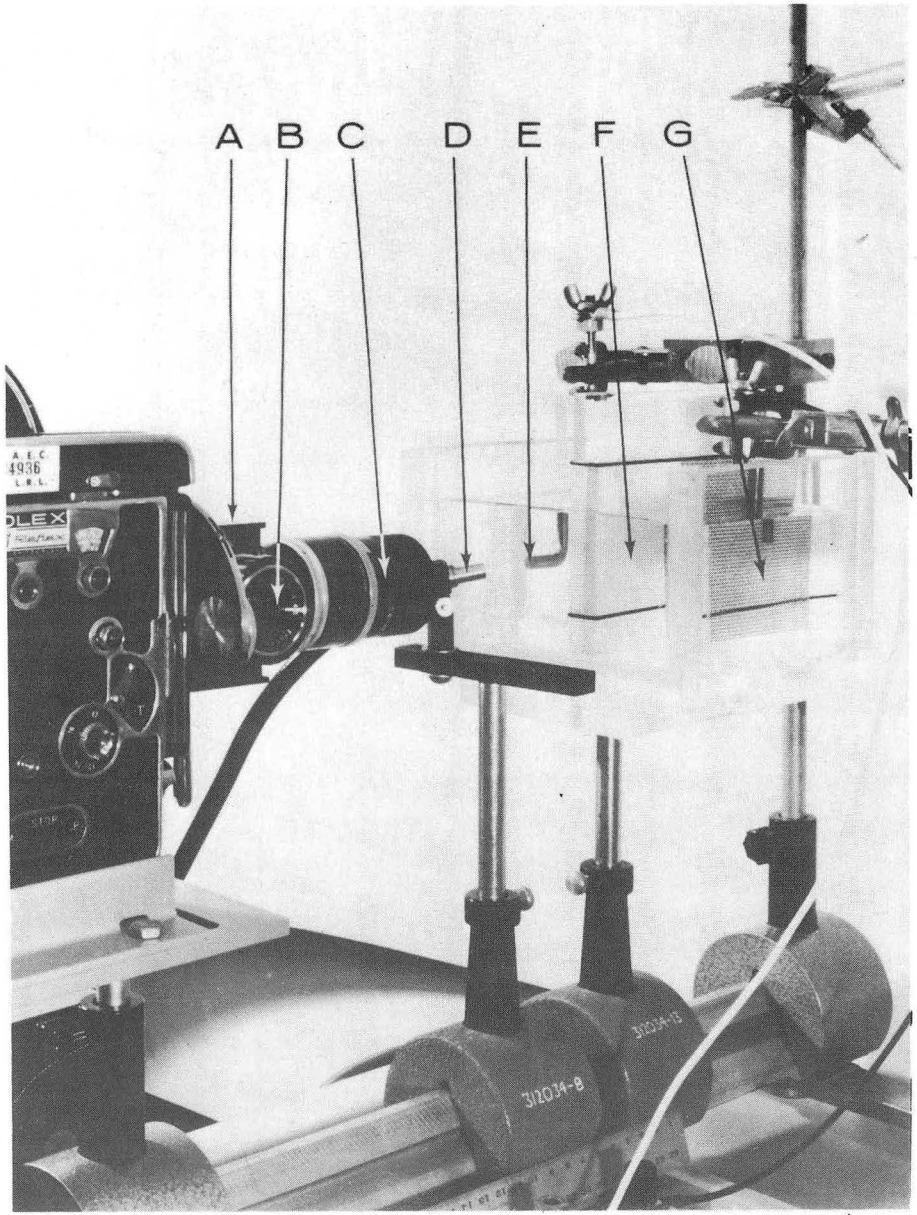

CBB 7011-5247A

Fig. 6. Stagnant cell apparatus. A. The beam splitter box. B. 90 mm Telesar lens directed toward pen recorder. C. 75 mm Switar lens directed toward the anode. D. Fiber optics guide for illuminating the anode. E. Anode (OFHC Copper). F. Porous nylon barrier. G. Cathode (stainless steel screen).

B. The Optical System

Another objective of this study was the correlation of visually observed phenomena occurring at the anode surface with cell voltage. This was achieved by the simultaneous superposition of an image from the anode with an image from a pen recorder trace on the same frame of film. The arrangement is illustrated in Fig. 7.

The filming speed was selected such that a particle moving at the bulk velocity in the flow channel would traverse the entire field of view, when projected at 24 frames/sec, in one second. This corresponded to a filming speed of 1,000 frames/sec for a linear flow velocity of 100 cm/sec. For experiments at very low flow rates, and in stagnant solutions, a 16 mm motion picture camera* was used with filming speeds of 32 and 64 frames/sec. The camera was driven by an electric motor while filming at 32 frames/sec for extended periods of time. The electric motor drive could not be used at 64 frames/sec. Instead, the spring drive was used, which limited filming sequences to about 8 seconds. For high flow velocities, a Hycam High-Speed Motion Picture camera was used with filming speeds up to 4,000 frames/sec.** (This model Hycam is capable of filming speeds up to 11,000 frames/sec.) Filming speeds were limited by the available illumination.

Since two different cameras were used for this study, it was necessary to build an optical system adaptable to either camera. A beam splitter box was constructed that provided mountings for the two objective lenses and a C-mount connection acceptable by either the

---

*H16 Rex camera, Bolex Paillard, Switzerland

**Model K2004E-115, Red Lake Laboratories, Inc., Santa Clara, CA. 95051

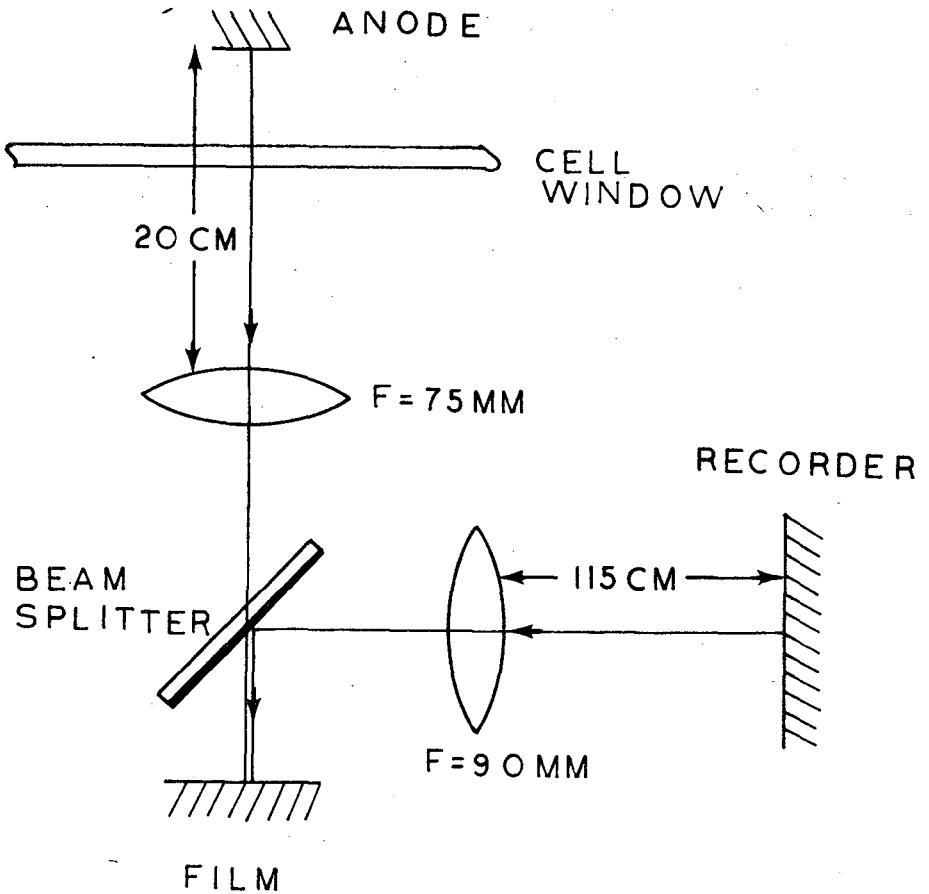

XBL 714-666

Fig. 7. Schematic diagram indicating the method of superimposing the recorder image and the anode image.

Bolex or Hycam. Inside the box, a mount held a partially transmitting mirror. (Part of the beam splitter box can be seen in Fig. 6.) The Bolex camera was bolted to a carrier mounted on a triangular optical bench. The Hycam was bolted to a 2.5 cm thick aluminum plate in place of the optical bench.

An f/1.9 Switar lens with a 75 mm focal length was used for observing the anode.* This was a normal, color-corrected, telephoto lens. The beam splitter box had the effect of an extension tube 62 mm long. With this combination, the ratio of the anode size to the image size, on the film plane, was very close to 1:1.

The anode image was transmitted through the beam splitter onto the film plane. Resolution was limited by the type film used. Ektachrome EFB film was selected for its combination of good color balance and high speed (A.S.A. 125).** The resolution limit of this film is about 36 lines/mm.[21] The resolution of the Hycam near the edge of the film was 56 lines/mm and at the center, 68 lines/mm.[22] With a resolution limit of 50 lines/mm and the largest aperture (f/1.9, used at the highest filming speeds), the depth of field was computed to be 0.2 mm. This agreed well with estimates made by observing bubbles in the electrolyte bouncing off the anode surface. The depth of field is inversely proportional to both the aperture and the magnification. For higher filming speeds, more illumination is needed, hence a larger aperture, and for smaller electrodes, a greater magnification is required, both resulting in a smaller depth of field.

---

* Kern-Paillard, Switzerland

** Type 7242 in 100 and 400 foot spools, Eastman Kodak Company, Rochester, New York

The lens used to focus the pen recorder trace on the film plane was an f/4.5 Telesar anastigmat enlarging lens with a 90 mm focal length.* The effective extension length of the beam splitter box was about 60 mm.

A beam splitter mirror was used to reflect the image of the recorder trace upon the film plane, while transmitting the anode image. The mirror was made from a microscope slide glass plate with a vapor deposited nichrome coating on the first surface and an antireflection coating on the second surface. For most experiments, a mirror with a transmission of 40 percent was used. The quality of the image from the recorder was slightly inferior to that from the anode due to a double image reflected from the second surface of the mirror, in spite of the antireflection coating. The image from the recorder was also reverse (left for right), but this was corrected by reversing the normal electrical connections and pen position on the recorder.

Illumination for the anode was provided by an Ealing Fiber Light Source.** The light source used a 150 watt tungsten-halogen lamp and transmitted the light through a 61 cm long by 6.35 mm diameter fiber optics bundle. The radiance output at the surface of the light bundle was about 3 watts/cm^2. The fiber bundle provided a high intensity white illumination but did not transmit infra-red radiation beyond a wavelength of 2.5 microns.

Illumination of the pen recorder was provided by two, 500 watt photoflood lamps.

---

* Edmund Scientific Co., 300 Edscorp Bldg., Barrington, N.J. 08007

** The Ealing Corporation, 2225 Mass. Ave., Cambridge, Mass. 02140

With the 40 percent transmission mirror, the image intensity at the film plane of the anode was about the same as that of the recorder (using the largest apertures on both lenses). Therefore, with the present system, filming speeds were limited by the reflected light from both the anode and the recorder. Filming speeds of up to 1,000 frames/sec have been used with success. With special color processing, having the effect of providing an additional two f-stops of illumination, filming speeds of 4,000 frames/sec could be used. However, the special processing resulted in some color shift and it was not able to fully compensate for the inadequate lighting.

A table of apertures and filming speeds used in this study is shown below.

Camera	Filming speed frames/sec	Aperture setting[a] 75 mm lens	90 mm lens
Bolex	32	f/8	f/11
	64	f/5.6	f/8
Hycam	1,000	f/1.9	f/4.5
	4,000[b]	f/1.9	f/4.5

a. focus set at infinity and illumination as mentioned in the text

b. with special processing

C. The Electrical System

The electrical system consisted of three sub-systems: a power source and sink, measurement and display circuits for the cell current and voltage, and a timing circuit for coordinating the operation of the various components.

A power supply capable of operating in either a constant current mode or a constant voltage mode up to 10 amperes at 120 volts d.c. was used.* Water cooled resistors were placed in series with the power supply. This had the effect of minimizing initial transients in the power supply and damping current fluctuations.

A two channel Mark II Brush Pen Recorder was used to display the cell voltage and current.** The surface of the recorder was masked with black velvet to permit just the voltage trace to be filmed. The input to the recorder for the current measurement came from the voltage drop across two precision resistors with ratings (within 1 percent accuracy) of 400 millivolts at 1 ampere and 400 millivolts at 10 amperes. Finally, a relay connected to the solenoid provided a signal to activate the event marker whenever the electrolyte was flowing.

Since it was necessary to trigger the various components in a definite sequence, a timer-relay system was constructed. A set of four, manually operated switches controlled: the light sources, a relay interupting power to the electrolysis cell, a remote starter for the camera, and a switch to actuate the timed relay, clock and electrolyte flow. Additional details and diagrams are included in Appendix A.

---

* Model KS120-10M, Kepco Inc., Flushing, N.Y.

** Model RD-2521-00, Brush Instruments, Division of Clevite Corp., Cleveland, Ohio

III. MATERIALS: METALS AND ELECTROLYTES

A. Metals

Metals used in this study were selected for either their metallographic significance (generally one or two component metals which have been extensively studied at lower current densities by previous investigators) or for their commercial importance (use in jet turbines and evidence that they were being commercially machined by ECM techniques). Six different metals were studied: high purity copper (99.99 and 99.999 percent), commercially pure nickel (99.5 percent), low carbon steel (0.18 percent carbon, SAE 1018), a nickel-copper alloy (MONEL K-500), and two nickel-base alloys (INCONEL X-750 and HASTELLOY HASTELLOY X). The copper, nickel and nickel-copper metals were selected primarily for metallographic reasons. The carbon steel and the two nickel-bases alloys were selected because of their commercial importance. The composition of these metals is given in Table I.

The anodes were fabricated from plates and rods; whichever mill product was readily available. Cutting to the desired configuration was done using standard machining techniques; milling, turning, grinding, etc. The finished anodes were then heat treated in an electric furnace and air atmosphere. The heat treatment procedures used on the fabricated anodes are tabulated in Table II. In the case of INCONEL X-750 and the carbon steel, where the heat treatment procedure would have resulted in prolonged exposure to air at high temperatures, the finished electrodes were placed in stainless steel bags during the heat treatment. There was a small amount of oxide on most of the heat treated alloys. The oxide was removed by sanding.

Table I. Composition of metals photographed during anodic dissolution.

Metal	Major components	Composition, percent										
		Ni	Cr	Fe	Cu	C	Si	Mn	Al	Ti		Others
High purity copper[e]	Cu				99.999							⩽2 ppm oxygen
OFHC copper[f]	Cu				99.99							
NICKEL 200[g]	Ni	99.0[a]		0.40[b]	0.25[b]	0.15[b]	0.35[b]	0.35[b]			0.01[b]	
SAE 1018[h] (low carbon steel)	Fe			98.9-99.16		0.15-0.20		0.60-0.90			0.050[c]	P=0.040[c]
MONEL K-500[i]	Ni-Cu	64.38		1.04	30.33	0.15	0.12	0.55	2.92	0.48	0.005	
INCONEL X-750[i] (age hardenable)	Ni-Cr-Fe	72.76[d]	15.65	7.09	0.04	0.05	0.18	0.11	0.74	2.42	0.007	Cb+Ta=0.91
HASTELLOY X[j]	Ni-Cr-Fe-Mo	balance (47.52)	20.50-23.00	17.00-20.00		0.05-0.15	1.00[c]	1.00[c]				Co=0.5-2.5 W=0.2-1.0 Mo=8.00-10.00

References to Table I

a. minimum value

b. maximum value, nominal composition is about half the maximum

c. maximum value

d. may include small amounts of Co

e. American Smelting and Refining, Central Research Labs, South Plainfield, New Jersey 07080

f. American Brass and Copper Company, Oakland, California 94623

g. Huntington Alloy (from stock at Lawrence Livermore Laboratory) Composition from "Handbook of Huntington Alloys," International Nickel Company, 1960, p.5.

h. SAE 1018 cold finished bars (from stock at Lawrence Berkeley Laboratory) Composition from Metals Handbook

i. Huntington Alloy, distributed by Pacific Metals, Division of A. M. Castle and Co., San Francisco, Ca. 94107. Certified chemical analysis supplied with the metal.

j. Stellite Division, Cabot Corporation, Kokomo, Indiana (from stock at Lawrence Berkeley Laboratory). Composition from "HASTELLOY alloy X," Cabot Corporation, 1970, p.3.

The finished metal electrodes were then cast in epoxy* (see Fig. 5). Finally, the surface to be observed during anodic dissolution was polished. Polishing was necessary to insure a hydrodynamically well defined surface and to aid in the observation of oxide layers formed during the initial period of dissolution.

The metals were first polished on a series of emery papers from 1/0 to 4/0; with kerosene as the lubricant. The copper electrodes were finished by polishing with 1.0 micron chromic oxide** followed by 0.5 micron chromic oxide*** on a polishing wheel. All other metals were finished using 1.0 micron diamond paste on a polishing wheel.**** Again, kerosene was used as the lubricant. After polishing, the metal surfaces were carefully cleaned using alcohol, acetone, and soap solution. Just prior to the experiment, the electrodes were again cleaned by hydrogen evolution at 1 ampere/cm^2 for one minute in 1N NaOH and rinsed with distilled water.

Figure 8 shows a surface profile of a polished electrode.***** In this case the electrode was made of nickel, but essentially the same profiles resulting from using the other metals. The electrode was inserted into a stainless steel holder during polishing to minimize rounding. Nevertheless, as can be seen in the figure, the surface was slightly rounded after polishing. For the nickel electrode shown,

---

* Shell Chemical Company, Epoxy 826 and Catalyst C-23 cast at room temperature from 65 percent (by weight) epoxy and 35 percent catalyst.

** AB Metpolish No. 1, Buehler Ltd., Evanston, Illinois

*** AB Metpolish No. 3

**** AB Metadi

***** Surfanalyzer model 150, Clevite Corporation, El Monte, Cal.

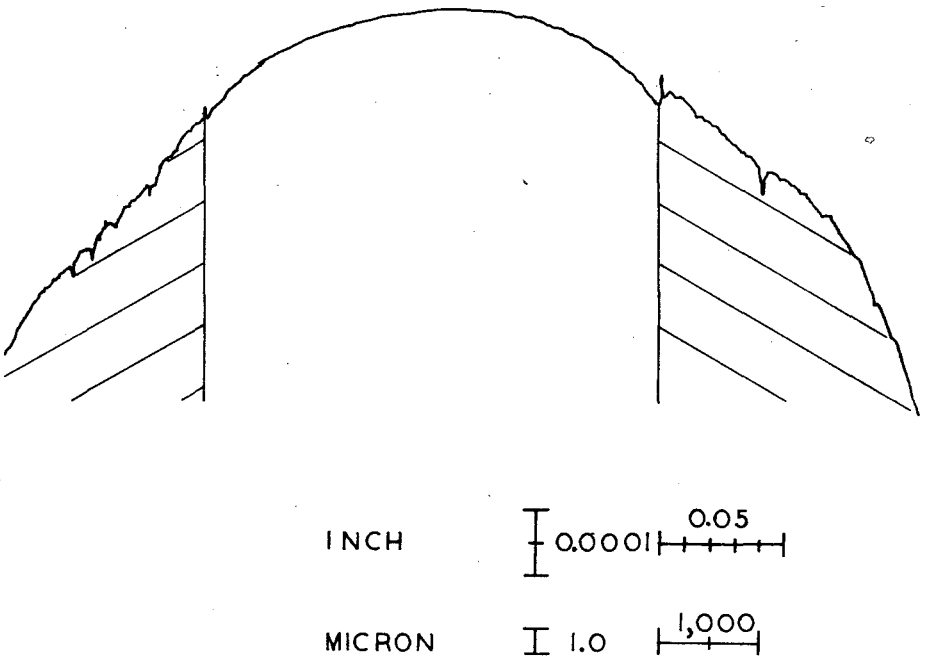

XBL 714-664

Fig. 8. Surface profile of a nickel anode after polishing. The cross hatched sections on the left and right are epoxy, in which the metal was cast.

the center of the bulge was about 4 microns above the plane of a flat surface. This slight elevation occurred on a surface 5,000 microns wide. The metal surfaces were generally much smoother than the adjoining epoxy and the gap between the epoxy and metal was very small.

1. Copper

Due to the relative wealth of data available for copper, as compared with more complex alloys, this metal was selected as the starting point for this study.

For the stagnant cell experiments, oxygen-free high purity copper (OFHC, 99.99 percent) in cold drawn rod form was used. This was the only metal studied in the stagnant cell shown in Fig. 6. In forced convection experiments, a high purity copper (ASARCO, 99.999 percent) was used. This copper had been recrystallized during manufacture, resulting in a grain structure visible to the unaided eye (mean diameter of crystals was several millimeters). The metals, both OFHC and ASARCO, were fabricated from the metal as received with a minimum of machining and were not heat treated.

2. NICKEL 200[23]

Electrochemical machining (ECM) is employed primarily for fabricating very hard, space-age metals that are basically high nickel content alloys. NICKEL 200, commercially pure nickel (99.5 percent), was selected for experiments to observe the behavior of the major constituent of the nickel-based alloys. The anodes were fabricated from cold rolled plate, then annealed.

3. Carbon Steel

In commercial operations, the ECM process is being used to machine low chromium steels (such as 5160H, 1 percent Cr) in the

Table II. Heat treatment procedures used on fabricated anodes.

Metal	Treatment Temp., °F	Treatment Time	Cooling	Remarks
High Purity Copper				Contained large crystals resulting from recrystallization.
OFHC Copper		none		Anodes fabricated from cold drawn rod.
Nickel 200	1600	5 min.	air cooled	Mean diameter of grain 0.071 mm max.; this is a medium grain size.[a] Anodes fabricated from cold rolled plate.
SAE 1018	1600	30 min.	furnace cooled to 1300°F at 50°F/hour	The full annealing procedure used for small carbon steel forgings was employed.[b] Anodes fabricated from cold finished plate.
MONEL K-500	1700	10 min.	water quenched	This is an annealing process. Anodes fabricated from cold drawn rod.[c]
INCONEL X-750	2100 1550 1300	2 hours 24 hours 20 hours	air cooled air cooled air cooled	Age-hardening process for high temperature service (above 1100F).[d] Anodes fabricated from cold rolled plate.
HASTELLOY X		none		Anodes fabricated from cold rolled plate.

References for Table II

a. "Huntington Nickel Alloys", Huntington Alloy Products Division, The International Nickel Company, Inc., p. 12.

b. Metals Handbook, 2, p.3.

c. "Monel Nickel-Copper Alloys", Huntington Alloy Products Division, The International Nickel Company, Inc., pp. 31-48.

d. "Engineering Properties of INCONEL alloy X-750" (Technical Bulletin T-38), Huntington Alloy Products Division, The International Nickel Company, Inc., p.9.

manufacture of complex shapes, such as gears.[24] SAE 1018 is a low-carbon steel (0.15-0.20 percent carbon), selected for qualitative observations of the behavior of iron at high current densities.[25] The carbon content is below that required for significant hardening of the metal by heat treatment.

4. MONEL K-500[26]

Since copper and nickel were being studied as pure metals, it was hoped that an alloy of the two would give some insight into the behavior of an alloy as a function of its chemical composition. This alloy contained about 65 percent nickel and 30 percent copper, with the remainder being mostly aluminum and titanium. As explained in the section for INCONEL X-750, aluminum and titanium with nickel may form a gamma prime phase and permit the metal to be age-hardened. It was considered desirable to maintain as uniform a composition as possible, without large grains. Therefore, the alloy was not age-hardened for this study.

Anodes were fabricated from cold drawn rod that had been partially flattened by cold rolling. The finished electrodes were annealed.

5. INCONEL X-750[27]

INCONEL X-750 is an age-hardenable nickel-chromium-iron alloy. Its high corrosion and oxidation resistance coupled with good mechanical properties (high creep rupture strength at temperatures up to 1500°F) have made it an important alloy for the fabrication of gas turbine rotor blades and wheels, jet engine afterburners, ramjets and rockets. It is a good example of those alloys that are difficult to machine by

conventional methods and which have been machined by ECM.

The alloy is made age-hardenable by the combination of aluminum and titanium with nickel to form gamma prime--the intermetallic compound $Ni_3(Al,Ti)$. After age-hardening, there is a linear contraction of the metal specimen on the order of 1/2 mil per inch (0.05 percent). In the commercial fabrication of parts with this alloy, the rough machining is often done on the unaged metal, followed by an age-hardening heat treatment, and then the final machining. With ECM processes it is possible to perform all the machining on the age-hardened alloy, since the cutting speed is determined by the electrochemical reactivity of the alloy, rather than its hardness.

The INCONEL X-750 samples used in this study were fabricated from hot-finished plate, then heat treated for high temperature service (above 1100°F). With this heat treatment on bars and plate, the sample should meet AMS specification 5668 which requires the following minimum rupture life:

100 hours at 1350°F and 45,000 psi

The specification also prescribes a stress increase to 70,000 psi, after 100 hours under the above conditions, and continuation of test until specimen fracture. Elongation after fracture, measured at room temperature, is required to be 5 percent minimum.

6. HASTELLOY X[28]

HASTELLOY X is another nickel-base alloy with excellent chemical and mechanical properties. However, this alloy does not contain aluminum and titanium, as in the case of INCONEL X-750, and is, therefore, not age-hardenable. Instead, it contains molybdenum as a primary

alloying element for resistance to chemical corrosion. This results in high strength and oxidation resistance to 2200°F. It is used in furnace applications (especially cracking furnaces in the petrochemical industry) and aircraft engine parts, such as afterburner components and nozzle vanes.

Anodes were fabricated from cold rolled plate. They were not heat treated.

B. Electrolytes

Most ECM processes use concentrated, neutral salt solutions as the electrolyte.[2] The electrolyte and concentration is chosen to minimize power losses, to obtain accurate machining, and to obtain a good surface finish.

The concentration selected to minimize power losses is a compromise, since concentrated solutions have a higher electrical conductivity, which reduces the IR power loss, but generally also have higher viscosities, which increase viscous losses. Solutions of potassium salts generally have a higher conductivity than solutions of sodium salts, but are more expensive.

Selection of an electrolyte for its machining and surface finish properties is still an art. Hoare, et al., investigating chlorate electrolytes, suggest good electrolytes produce a moderately protecting film on the workpiece and a sharp transition from the passive to the transpassive state.[10] Chin and Wallace have presented a new way of using a modified Haring-Blum cell to determine a throwing power for ECM electrolyte.[29]

In this study, it was decided to use the three most common ECM electrolytes: sodium chloride, sodium nitrate, and sodium chlorate. 5N solutions were used, as representative of concentrated solutions normally found in industry, and as a common concentration for all the electrolytes. Among ECM electrolytes, sodium chloride (NaCl) is one of the most common salts, because it is obtainable in fairly pure form at low cost ($6.50/100 pound quantities of technical grade salt). Sodium nitrate ($NaNO_3$) is more expensive ($13.95/100 pounds), but often results in a much better surface finish for most metals than results when using sodium chloride. Perhaps the best electrolyte, based on surface finish and accuracy of cutting, is sodium chlorate ($NaClO_3$).[10] This is also the most expensive ($21.60/100 pounds) of the commonly used salts.

For the stagnant cell experiments and a limited number of forced convection experiments, 2N solutions of reagent grade potassium salts were used so that the observed results could be compared with those of Kinoshita.[14] For the flow channel experiments with various alloys, 5N solutions of technical grade salts were used. The technical grade solutions were filtered through No. 1 Whatman filter paper to remove suspended dirt. In all other respects, the materials used were the same as in industrial ECM.

Standard silver titrimetric tests for chloride concentration were performed on the technical grade sodium nitrate and sodium chlorate solutions.[31] The concentration of chloride ion was found to be about 0.016N in 5N sodium nitrate and 0.01N in 5N sodium chlorate. The sodium chlorate also had a pale yellow color due to dissolved iodine (I_2). Although some difficulty was encountered in the titration

(the standard starch test), the concentration of iodine was measured to be about 0.005N.[31] The sodium chloride solution was filtered to remove magnesium carbonate precipitate and the resulting solution was assumed to be saturated in magnesium carbonate at a level below 0.005N.[32]

The low volumetric flow rates used with these electrolytes made it unnecessary to recycle any electrolyte, thus avoiding a buildup of reaction products.

Physical properties of the solutions are tabulated in Table III and in Appendix B.

Table III. Electrolyte properties for 5N solutions at 25°C.

Compound	Molecular Weight g/g-mole	Density g/cm^3 Exp.[a]	Density g/cm^3 Lit.[b]	Viscosity centipoise Exp.[c]	Viscosity centipoise Lit.[d]	Molar conductance Ω^{-1} cm^2/mole	Weight percent[g]	Solubility* o/o[h]	Solubility* N[i]
NaCl	58.45	1.195	1.184	1.69	1.64	49.46[e]	24.5	26.48	5.4
$NaNO_3$	85.01	1.266	1.257	1.63	-	38.7[f]	33.6	47.92	7.8
$NaClO_3$	106.45	1.335	1.318	1.87	-	-	39.9	51.7	7.0

* Solubility for saturated solutions

References for Table III

a. Experimentally determined using a 25 ml picnometer and technical grade solutions

b. International Critical Tables

c. Experimentally determined using an Ostwald viscometer and technical grade solutions

d. International Critical Table

e. Chapman and Newman, p. 246 cites: Chambers, Stokes and Stokes. J. Phys. Chem., 60, 985 (1956) see ref. 30

f. Extrapolated from data in Chapman and Newman, p. 267 cites: Gellings. Rec. Trav. Chim., 75, 209 (1956)

g. Computed from experimentally determined densities

h. International Critical Tables

i. Computed from data in International Critical Tables

IV. RESULTS

Included in this section are summaries of the observations made during the anodic dissolution of copper, nickel, carbon steel, MONEL K-500, INCONEL X-750, and HASTELLOY X in NaCl, $NaNO_3$, and $NaClO_3$ electrolytes. Tables IV to VII tabulate the observations of solid and gaseous reaction products at 1 and 20 amperes/cm^2 in forced convection (electrolyte flow velocity of 10 cm/sec). The measured overall cell voltages recorded during high and low current density dissolution are listed in Table VIII. Also included are brief descriptive accounts, especially for copper which was studied in both free and forced convection.

In general, there were more similarities among experiments using the same metal in different electrolytes than with the same electrolyte with different metals. Therefore, the summaries of observations are given first for each metal, then for the electrolytes.

The primary experimental data are contained on 3,100 feet of motion picutre film. A list of the dissolution events filmed is included in Appendix C.

Table IV. Anodic gas evolution observed during low current density dissolution.[a]

Metal	Electrolyte[b]		
	NaCl	$NaNO_3$[c]	$NaClO_3$
Copper	no gas	no gas	gas[g]
Nickel	no gas	gas[d]	gas[d]
Carbon Steel	no gas	gas[d]	gas[d]
MONEL K-500	no gas	gas[e]	gas[h]
INCONEL X-750	no gas	gas[f]	gas[d]
HASTELLOY X	no gas	no gas	no gas

a. 1 ampere/cm^2 and a flow velocity = 10 cm/sec

b. 5 normal solutions prepared from technical grade salts

c. There was practically no cathodic hydrogen observed for any of the experiments at 1 ampere/cm^2 conducted in $NaNO_3$.

d. The most commonly observed form of gas evolution was that of a layer of bubbles of uniform size which covered the entire anode surface. The volume of evolved gas appeared to be greater in $NaClO_3$ than in $NaNO_3$.

e. Very small bubbles observed on the entire surface during dissolution.

f. For about 0.1 sec after the beginning of dissolution, gas was produced only at grain boundaries, then gas began to evolve uniformly over the entire anode surface.

g. Bubbles observed after a solid green layer peeled from the surface.

h. A small number of small bubbles observed on the electrode surface during dissolution.

Table V. Anodic gas evolution observed during high current density dissolution.[a]

Metal	Electrolyte[b]		
	NaCl		$NaClO_3$
Copper	small[c]	medium[f,l]	medium[i]
Nickel	medium[d]	large[g,l]	large[g,l]
Carbon steel	small[d]	large[h,k]	large[g,l]
MONEL K-500	medium[d,k]	large[c,k]	large[c,j]
INCONEL X-750	medium[d,k]	medium[c,j]	large[c,l]
HASTELLOY X	medium[e]	small[d]	medium[c,j]

a. 20 amperes/cm^2 and flow velocity = 10 cm/sec. Gas evolution was observed in all experiments. However, the volume of gas and the size and distribution of bubbles varied greatly among the metal/electrolyte combinations. An estimate was made of the relative volumes of gas produced, on the scale: small, medium and large. "Small" gas evolution corresponded roughly to the highest gas evolution rates observed at 1 ampere/cm^2.

b. 5N solutions prepared from technical grade salts.

c. The gas evolved uniformly covered the entire surface.

d. Gas evolved as a "horseshoe" pattern with most of the gas along the two side edges and trailing edge of the anode. Very little gas evolved at the leading edge or center of the electrode. The color of the central and outer edges of the anode often indicated that different solid reaction products were produced in the gas evolving and non-evolving regions.

e. The "horseshoe" pattern (see d.) changed to a "layer" of bubbles of uniform size evolved on the entire anode surface.

f. Gas evolved only along the trailing third of the electrode.

g. "Pulsating" gas evolution. Normally, the gas began by evolving in the "horseshoe" pattern. However, at high rates of gas evolution the bubbles coalesced into one large bubble. These bubbles were swept away fairly regularly, hence, the pulsating effect.

References to Table V, continued

h. Normally, the major portion of the evolved gas was swept downstream directly behind the electrode. In this particular case, substantial volumes of gas were also swept to the sides of the electrode, forming a parabolic gas profile with the opening of the parabola facing downstream.

i. Bubbles with diameters larger than in any other experiment were evolved at the anode and cathode. Periodic potential oscillations, normally characteristic of the copper/chlorate system, were not observed during this experiment (see text for details of oscillations and references).

j. Very small oscillations, less than 1 volt, that showed little relation to the evolved gas patterns.

k. Small potential oscillations, approximately 2 volts.

l. Large potential fluctuations, greater than 5 volts, occurring in experiments where the anode was covered by large volumes of evolved gas.

Table VI. Reaction products observed during low current density dissolution.

Metal	Electrolyte		
	NaCl	$NaNO_3$	$NaClO_3$
Copper	A white layer of solid products, with pores, through which dark brown solids oozed. The pores formed and were clogged randomly over the surface. Grains were visible during the initial iris.	A very thin layer of solids that peeled off in sections on the order of 0.5 mm. The grains were visible through the solid layer during dissolution.	Periodic shedding of solid layers. The initial white layer turned brown, then green and peeled off. The grain pattern was visible during the initial iris of the first layer produced.
Nickel	A solid layer of white and gray that did not cover the surface uniformly; the surface appeared to be granular. The iris pattern was not clearly visible.	A thin white layer covered the entire surface, with some dark brown reaction products produced near the edges.	Rust color solids and colored solution mixed with evolving gas.
Carbon steel	A white solid layer initially formed over the entire surface. There was a faint brown secondary iris.	No solid reaction products were observed. The evolution of gas obscured any solids there may have been.	Gas evolution on most of the surface. Rust colored solids observed along the edges and at the leading corners of the electrode. The remaining surface did not appear to have been dissolved; scratches from polishing remained.

Table VI, continued

Metal	Electrolytes		
	NaCl	$NaNO_3$	$NaClO_3$
MONEL K-500	A uniform layer of grey solids was produced on the surface. The iris pattern was visible, but faint.	Layer of white solid reaction products formed on the surface.	A white layer of solid reaction products was observed, with many very fine particles swept along the anode edges and downstream.
INCONEL X-750	The initial layer consisted of yellow solids, but gradually turned white as dissolution continued. After dissolution an etched surface was clearly visible.	An initial layer of gas bubbles which suddenly stopped evolving to reveal an etched surface. An iris of yellow reaction products then formed.	Dissolution appeared to be primarily along the anode edges. An etched surface was revealed after dissolution.
HASTELLOY X	A series of faint irises of different colors quickly formed. Then, a viscous layer of yellow solid products was produced, that slowly washed off the surface.	Yellow solid reaction products were produced. These products appeared to peel off the surface.	Yellow solid reaction products were produced. The layer did not peel, but instead, slowly washed off as fine particles.

Table VII. Reaction products observed during high current density dissolution.

Metal	Electrolyte		
	NaCl	$NaNO_3$	$NaClO_3$
Copper	Yellow and brown solid reaction products were produced in finely divided non-adhering form.	Initially the reaction products were dark red. This gave way to straw colored solid particles as dissolution continued. Gas was observed to be emitted from pores(?) on the layer of solid products.	Primarily green, solid fluffy products, with traces of yellow and brown. The initial dissolution revealed very quick iris patterns.
Nickel	Fluffy green solids that appeared to be shed periodically. These solids did not form cohesive layers.	No solid products were observed. The surface after dissolution revealed a pattern of very fine etching.	Brown and black solid products, mixed with large amounts of evolved gas.
Carbon steel	Rust and red color solids produced in the center of the anode, gold color solids and gas evolved along the edges of the anode.	Initial solids were yellow color, but were quickly obscured by evolving gas. The surface after dissolution was a light gray color, as if sand blasted.	Small amounts of rust colored solids produced, but continued production was obscured by large volumes of evolved gas.

Table VII, continued

Metal	Electrolytes		
	NaCl	$NaNO_3$	$NaClO_3$
MONEL K-500	Black solids produced in the center of the anode, and gold color solids and gas produced along the edges. Pits were observed during and after dissolution	Fluffy green solid products, which were produced mostly at the center of the anode.	Primarily green fluffy solids with traces of white solids were observed. Pits were visible on the anode surface.
INCONEL X-750	Dark green solids produced in the center of the electrode, and yellow solids over the remainder.	Fine black particles produced over the entire surface. These were mixed quite uniformly with the evolving gas.	Initially, rust color solid products were produced. This quickly gave way to the production of black particles as in nitrate solutions.
HASTELLOY X	Black solids were produced in the center and yellow solids along the edges of the anode. The solution appeared to be light green in color.	Red solids were produced in the center and gold color solids along the edges.	Gold color solids were produced on the entire anode surface.

Table VIII. Steady state overall cell voltages measured during high and low current density dissolution.

Metal	Electrolyte					
	NaCl		$NaNO_3$		$NaClO_3$	
	1 A/cm^2	20 A/cm^2	1 A/cm^2	20 A/cm^2	1 A/cm^2	20 A/cm^2
Copper	15.5	28	2.4	30	4.0[d]	31
Nickel	3.5	a	4.3	b	4.3	40[c]
Carbon Steel	2.2	24	3.9	34	4.8	40[c]
MONEL K-500	2.5	24	3.4	23	6.2[e]	26
INCONEL X-750	2.8	b	3.5	21	4.4	27
HASTELLOY X	3.4	23	3.4	19	3.9	26

a. Greater than 20 volts

b. Greater than 8 volts

c. Greater than 40 volts

d. 4.0 volts initially with a peak at 6.2 volts

e. 4.0 volts initially with a slight inflection and a peak at 6.2 volts.

A. Copper

1. Free convection

As pointed out previously (see Section II. A. 2. The stagnant cell), the stagnant cell apparatus was used for preliminary experiments with OFHC copper. One overall objective of this study was to conduct the anodic dissolution under hydrodynamically well defined conditions. The stagnant cell was poorly suited for this purpose. Nevertheless, some interesting observations were made in free convection, and these are considered here.

The transition from an active to a transpassive state was observed in four electrolytes; the corresponding overall cell voltages are tabulated below.

Electrolyte	Overall cell voltage[a]	
	active	transpassive
2N KNO_3	7	30
2N KCl	5	20
1N K_2SO_4	10	40
2N $NaClO_3$	10	15[b]

a. current density = 3.15 amperes/cm^2

b. total cell voltage showed periodic oscillations between 10V and 15V; i.e., 5 volt fluctuations

The active/transpassive transition was indicated by one or both of the following events: (1) the completion of growth of a layer of solid reaction products that began at the edge of the electrode and grew toward the center, and (2) simultaneous with the completion of the solid layer, a step increase in the measured overall cell voltage. The appearance of the production of solids growing in the radially

inward direction suggests the term "iris effect", which will be used when referring to this phenomenon of solids growth.

In some electrolytes, several different irises were observed moving sequentially from the edge to the center. For example, copper in chlorate showed an initial formation of a white iris, followed by a pale yellow iris, then another iris with a dark brown color. In general, the iris patterns appeared only once, during the initial stages of the dissolution. With the copper/chlorate system, the iris patterns repeated periodically, as will be described more fully later. After the iris patterns were completed and the surface was covered with solid reaction products, gas started to evolve. This transition from a regularly growing solid layer to the evolution of gas was marked by a rapid change in the cell voltage. The low voltage region will be referred to as the "active mode" and the high voltage region the "transpassive mode".

The reaction products observed for copper in free convection were visually identical with those observed in forced convection (see Tables IV and V). In addition, copper was dissolved in 1N K_2SO_4, where the reaction product was a finely divided, very black powder.

Gas evolution was easily observed in free convection since the electrolyte did not sweep the bubbles off the surface, as was the case in forced convection. Motion picture photographs of the dissolution events were projected onto a screen where the events could be analyzed in single frame sequences. By measurements on these projected photos, the number and size of the bubbles evolved could be determined, and from this, an estimate was made of the volume of gas liberated. During the dissolution of copper in nitrate and sulfate (at 3.15

amperes/cm^2), bubbles were observed with diameters ranging from about 0.1 mm to 0.5 mm and were produced at a rate of 10 to 20 bubbles per second; this corresponds to 10^{-4} to 10^{-5} cm^3/sec. This rate of gas evolution, if assumed to be oxygen, could be produced by about 0.1 to 1 percent of the total current used in this experiment. (This subject is treated more fully in Section V.D. Evolution of gas.)

In all electrolytes except 2N KCl, gas evolution was observed for experiments performed in stagnant solutions at 3.15 amperes/cm^2. In a 2N $NaClO_3$ solution the gas appeared between successive layers of precipitate. In 2N KNO_3 and 1N K_2SO_4, the gas appeared as bubbles adhering to the juncture between the copper anode and the insulating varnish and appeared to be produced mostly along the outer edge of the electrode.

Side observations of the anode during dissolution in nitrate and sulfate solutions (at 3.15 amperes/cm^2) also revealed sudden emanations, or "jets", of reaction products from the anode surface. It was difficult to observe the "jets" while viewing the surface of the anode from the front. Side views revealed the emanations much more clearly, however, the restricted depth of field limited the observations to a smaller region of the electrode. The "jets" had a measured velocity of 1-2 cm/sec in nitrate solutions and about 3 cm/sec in sulfate solutions. Two or three emanations were observed during one 10 second experiment and these extended 8 to 10 mm from the anode surface before being mixed into the electrolyte. A study of front and side views seems to indicate that the "jets" were produced at the juncture between the copper and the insulating varnish. This is also the region where most of the gas was produced.

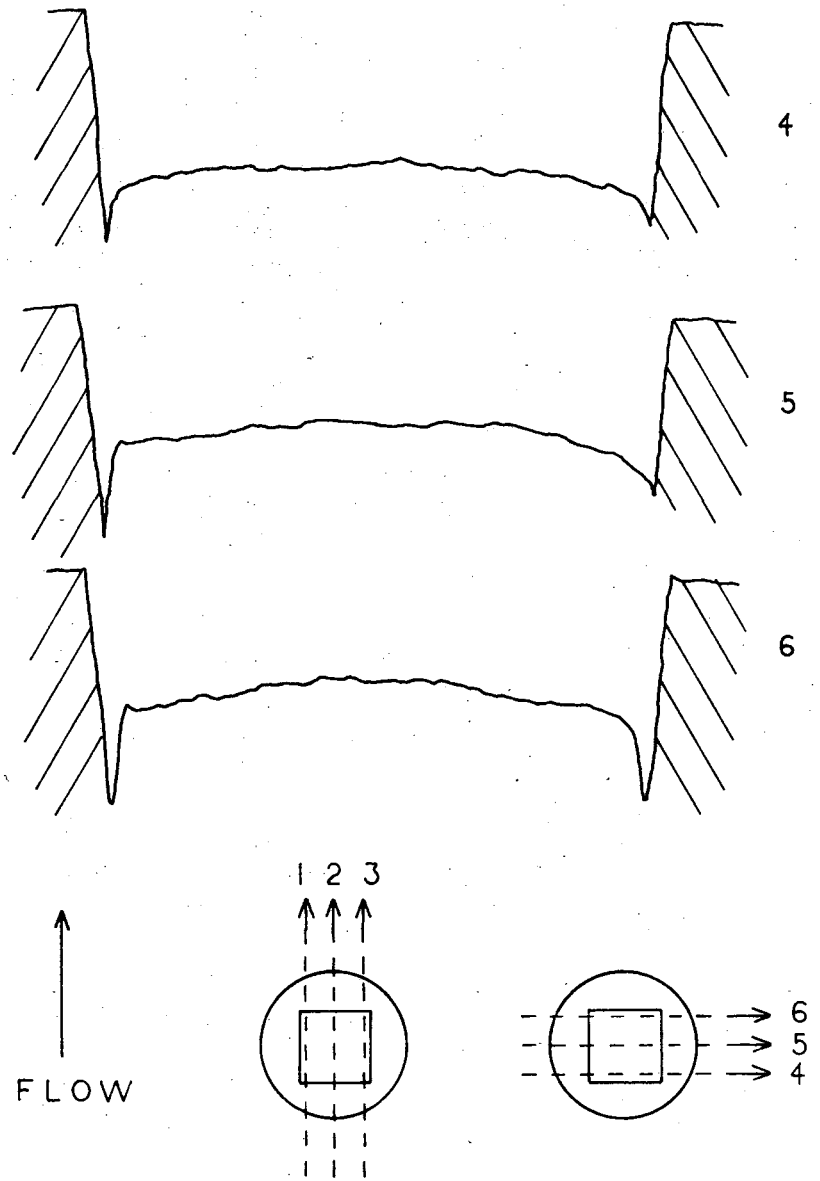

XBL 714-661

Fig. 11B. Surface profiles, continued. The figure above indicates the orientation of the profile with respect to the electrolyte flow.

Flow conditions	Current density ampere/cm^2	Oscillation period sec/cycle average	range	No. of experiments
stagnant	3.15	0.552	0.500-0.625	7
10 cm/sec	1.0	8.0	-	1
10 cm/sec	20	no oscillations		1
25 cm/sec	4.0	0.240	0.227-0.250	3
40 cm/sec	4.0	0.465	0.448-0.485	2

There is not enough data in the above table to justify making general statements about the relationship between the current density or flow velocity and the period of the oscillations. These data do agree, in general, with the more extensive data reported by Cooper, et. al.[33]

As mentioned earlier, copper in chlorate showed the sequential formation of a white layer (or iris), followed by a pale yellow layer, then a dark brown layer. When the dark brown layer peeled off, it rapidly changed from brown to a green color. Between the time one layer peeled off and the next layer formed, a small amount of gas was evolved uniformly across the surface. The sequence of irises began again during the gas evolution and ended with another layer peeling off. In some stagnant solution experiments, gas bubbles produced between the layers seemed to produce holes in the next layer. With 1/8 inch diameter copper electrodes in free convection, the initial layers were very uniform and seemed to adhere to the electrode. Some of these layers developed cracks as gas between the layer and the electrode pushed outward. Other layers possessed enough mechanical integrity to pop off the electrode as a whole and settle to the

surface profiles were not reliable indicators of the depth of the pores (even if it were possible to follow the stylus so one would know when it encountered a pore). Focusing methods, such as those used to produce Figs. 9 and 10, give a value for the pit depth of the order of several microns. The pores were about 30 microns from center to center and covered the surface with a density of about $10^5/cm^2$.

No pits were observed when OFHC copper was dissolved in 2N KNO_3 in free convection.

Figures 11A and B are surface profiles of the same copper electrode shown in Figs. 9 and 10; for comparison, Fig. 8 illustrates a nickel electrode surface profile before dissolution. The vertical and horizontal scales differ by a factor of 10, so the depth of dissolution appears exaggerated. Approximately 100 to 150 microns were dissolved. At lower current densities the amount of dissolution was considerably less. Nevertheless, these profiles are typical of the electrode surface for most of the metals after dissolution.

Chlorate

Kinoshita first reported the occurrance of periodic voltage oscillations when copper was anodically dissolved in chlorate solution.[14] This is of particular industrial interest because chlorate solutions have been shown to result in machining accuracy and surface finishes superior to most other electrolytes.[10] The relationship (if any) between the periodic phenomena and machining properties is not known. A table of observed periodicities, in the channel used for the present study, follows.

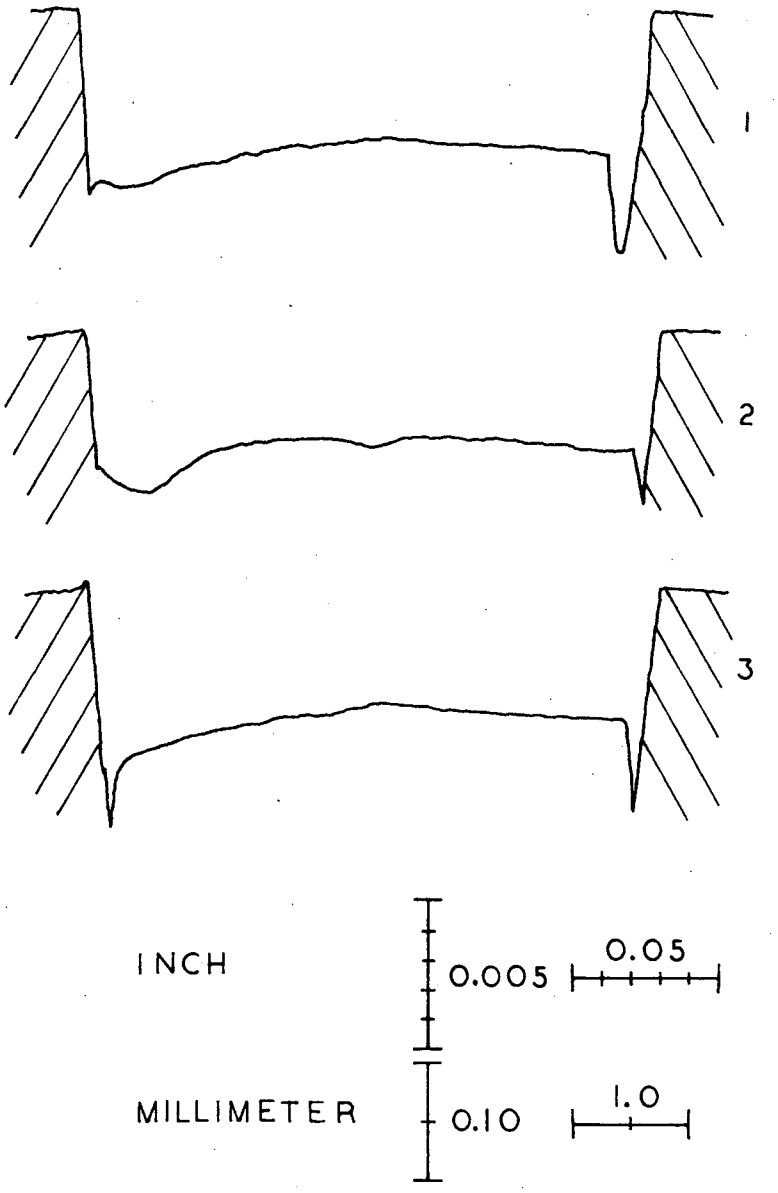

XBL 714-665

Fig. 11A. Surface profiles of a copper electrode after dissolution at 40 ampere/cm^2 in 2N KNO_3 and 150 cm/sec. The cross hatched regions on the left and right sides represent the epoxy, and the region between is the copper electrode. The slight slant in the walls of the epoxy is due to stylus error and not to the actual shape of the electrode. The leading edge is on the left and the trailing edge on the right.

2. Forced convection

The copper used in forced convection experiments was recrystallized (ASARCO, 99.999 percent) and had grains up to several millimeters in diameter. During the growth of the initial iris, the individual grains were very clearly visible. This behavior was not observed with OFHC copper used in free convection. Further considerations of this will be postponed until it can be discussed in relation to etching observed with other metals (Section V.C. Formation of solids).

Chloride

When copper was anodically dissolved in chloride, an initial white layer covered the surface. As the dissolution continued, at current densities around 1 ampere/cm^2, pores developed in the solid layer covering the electrode. Pale yellow reaction products oozed through a pore for a short time until the pore clogged up and a new pore developed at another point. At 3 to 4 amperes/cm^2, copper went into solution as a soluble copper complex, and very few solids were observed. However, the Schlieren pattern produced by concentration gradients was often observable. When the current density was still higher, 20 amperes/cm^2, yellow and brown solid reaction products were again formed, this time with the evolution of a moderate amount of gas.

Nitrate

One of the most interesting phenomena was the formation of pores or pits extending through the copper oxide film into the copper metal surface, during dissolution in nitrate solutions. Small pores were observed, with the aid of a microscope, after dissolution at 1 ampere/cm^2, when only a few microns of copper had been removed.

More pronounced pores, deeper and more uniformly distributed, were observed after dissolution at 20 amperes/cm^2 (flow velocity of 10 cm/sec and 40 amperes/cm^2 (flow velocity of 150 cm/sec) where the amount of copper dissolved was much greater, up to 150 microns.

Figures 9 and 10 are photographs (at a magnification of 200X) of the copper surface after dissolution at 40 amperes/cm^2 in 2N KNO_3 flowing at a velocity of 150 cm/sec. These two photos are of the same section of the electrode, but differ in the plane of focus. In Fig. 9 the microscope was focused at the bottom of the pits and in Fig. 10 the focus was on a plane above the electrode surface.

The photographs reveal a regular array of "pores" or "pits" and "grains" in the solid layer covering the copper electrode. Study of similar photographs of copper after dissolving at 20 amperes/cm^2 (flow velocity = 10 cm/sec in 5N $NaNO_3$) showed bare spots where the solid products had flaked off. In these regions, the array of pits was observed in the copper metal and would seem to indicate that the pores were not restricted to just the surface layer. However, the electrodes dissolved in an electrolyte flowing at high velocities had regions near the center of the electrode where the oxide layer was very thin, as judged from interference fringes. In these regions, there were no pits in the metal, although there were a few very shallow depressions. Therefore, for this type of pitting to occur, as shown in Figs. 9 and 10, a layer of solid reaction products, probably an oxide layer several microns thick, seems to be necessary. The depth of the pits and the thickness of the oxide varied across the electrode surface; from the poreless regions at the center to uniform areas of thick oxide near the edges. Due to the small size of the pores,

XBB 712-771A

Fig. 9. High purity copper after dissolution in 2N KNO_3 40 ampere/cm^2. Focus is on the bottom of the pits (200X).

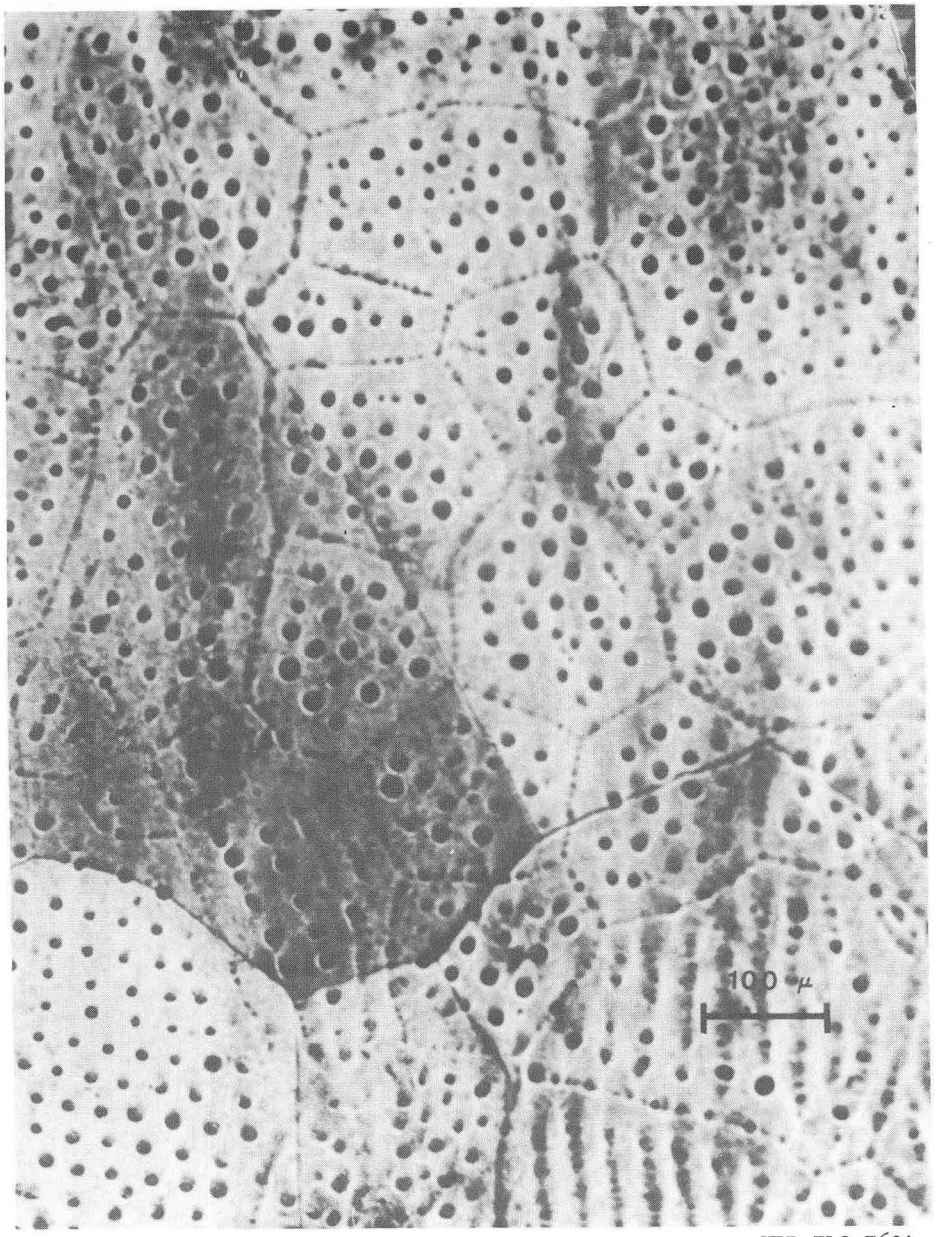

XBB 712-769A

Fig. 10. High purity copper after dissolution in 2N KNO_3 at 40 ampere/cm^2. Focus is on the plane above the surface (200X).

bottom of the stagnant cell. With stagnant solutions, the reaction products often accumulated at the electrode surface, preventing the observation of the successive growth of layers on the surface. In forced convection the layers were easily visible, but did not seem to have the same mechanical cohesiveness as the layers in free convection. The voltage oscillations were equally regular in both systems. In all cases where the iris development was visible, the voltage remained constant during the first two irises, rose suddenly during the last iris, and dropped suddenly as the green layer peeled off. There was no discernable difference between the behavior of OFHC (99.99) and ASARCO (99.999) copper.

Figure 12 is a photograph of a high purity copper electrode after dissolution in $NaClO_3$ at 1 ampere/cm^2. The current was turned off just as the voltage oscillations reached a peak and the layer peeled off. The photo shows the center of the electrode, where another iris was beginning to form. The motion picture films always showed an iris progressing from the edge of the electrode to the center, and the photo suggests the possibility of a number of pores or nucleation sites within an iris. The photograph has a magnification close to that used in Figs. 9 and 10. However, chlorate solutions never produced the type of pores observed with dissolution into nitrate solutions.

B. Nickel

With nickel, the nickel-based alloys, and carbon steel, the experimental observations were of an exploratory nature. Hence, fewer experiments were made than for copper. Most of the observations of solid and gaseous reaction products are listed in Table IV - VII and

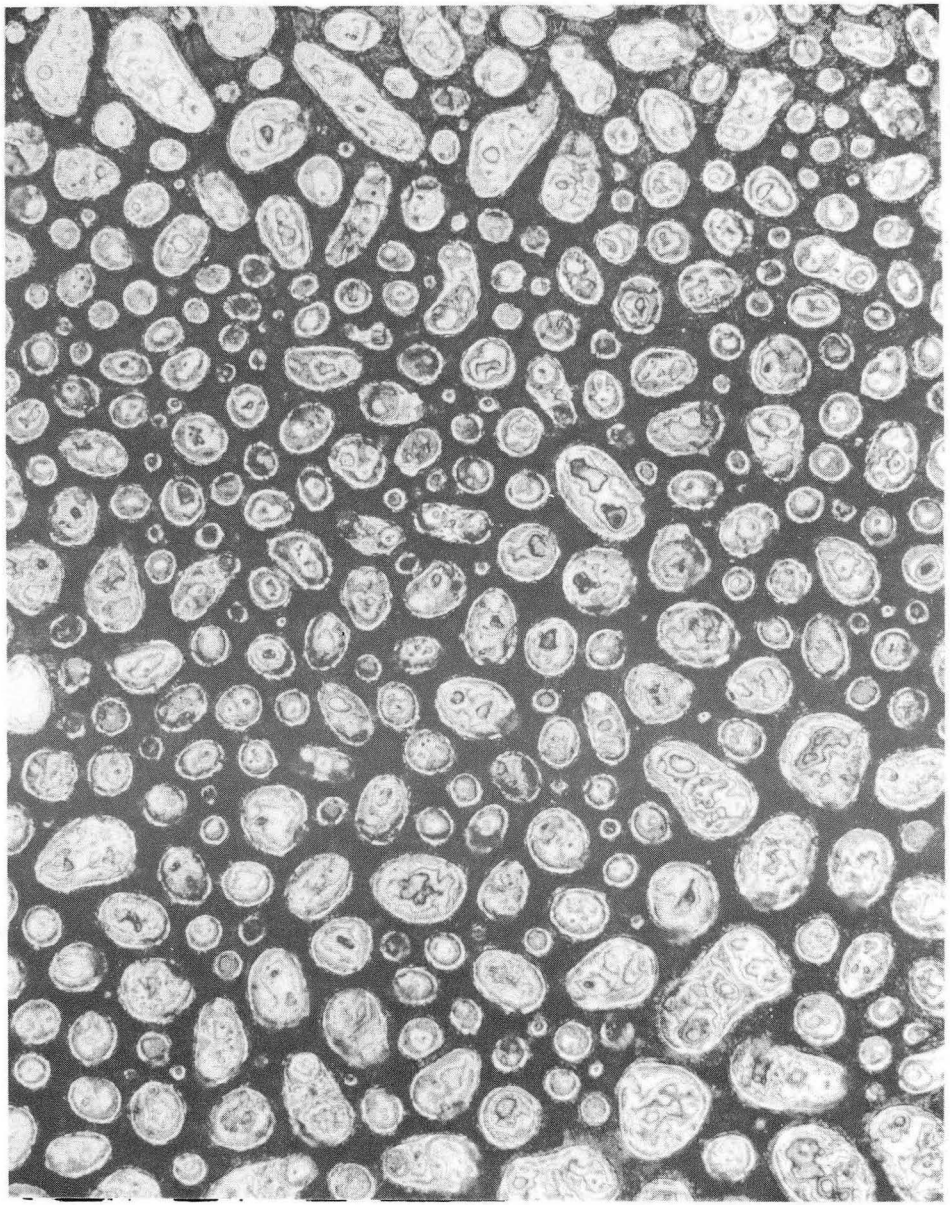

XBB 716-2508

Fig. 12. Copper surface after dissolution in 5N $NaClO_3$ at 1 ampere/cm^2. (Magnification of 160X, sample area is 0.690 mm × 540 mm)

the measured cell voltages in Table VIII.

The dissolution of nickel resulted in much larger volumes of gas than that observed during the dissolution of copper. This gas, by obscuring the anode surface, rendered observations and conclusions concerning the formation of solids unreliable. The evolved gas both shielded the anode surface from direct view and mixed with the reaction products. At high current densities, the layer of gas on the anode appeared to be at least a millimeter thick.

The reaction products observed were predominantly brown-black or sometimes rust color and appeared to be solids and concentrated solutions of metal salts. After dissolution, the anodes were often covered with a uniform flat gray-colored layer, probably an oxide. Figure 13 shows such a surface, with a few bright points in the layer. These bright spots appeared to be places where the surface layer had flaked off, thus exposing the underlying metal.

The cell voltages showed no active/transpassive transition. At high current densities, where voltage fluctuations were recorded, these appeared to be due to gas evolution.

C. Carbon Steel

Carbon steel was similar in its anodic behavior to nickel. Like nickel, large volumes of gas were evolved and this gas obscured the anode surface from direct observation. Fluctuations of the cell voltage due to gas evolution were the same as those with nickel. The reaction products ranged in color from gold to rust color. Also, like nickel, the products appeared to be a mixture of solids and concentrated solutions of metal ions.

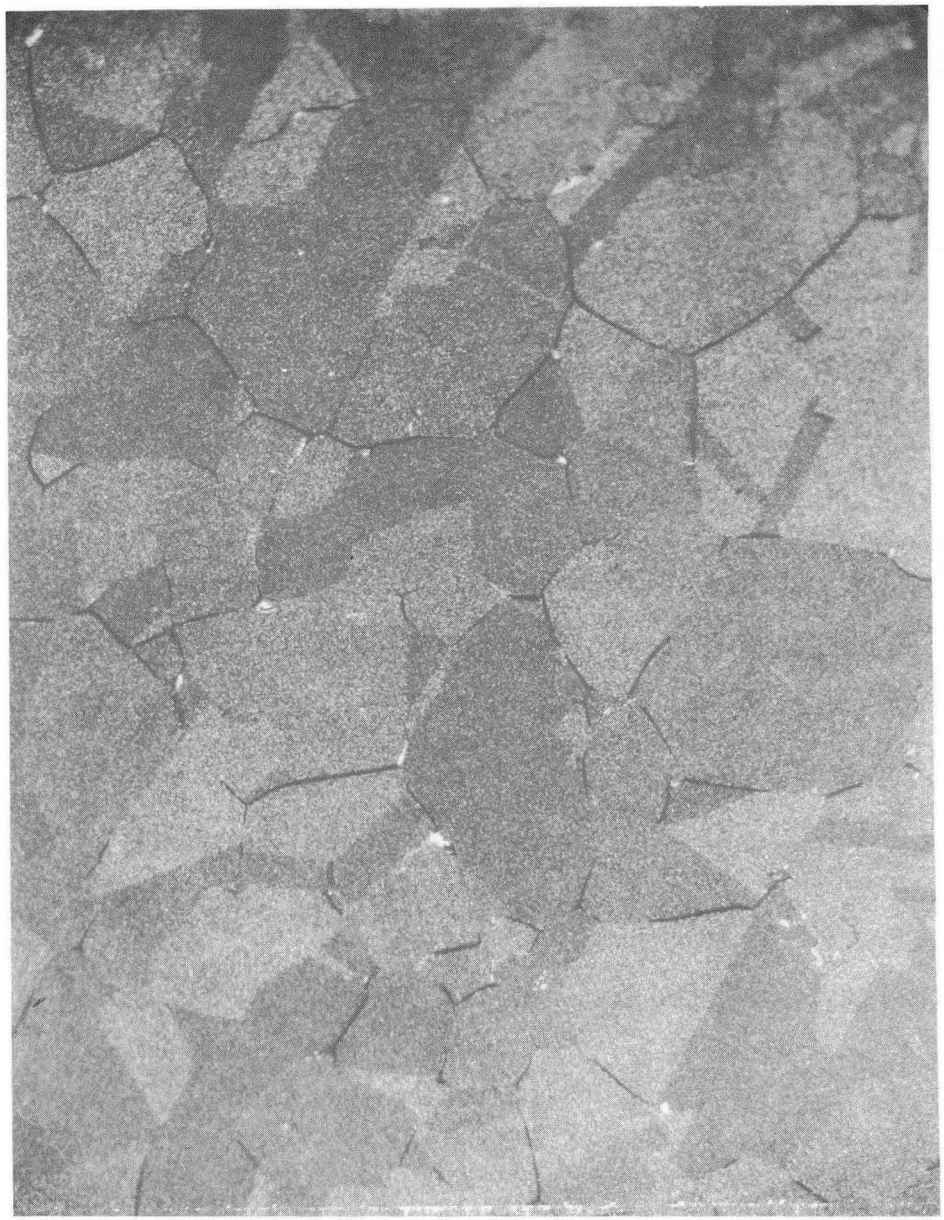

XBB 716-2504

Fig. 13. Nickel after dissolution in 5N $NaNO_3$ at 20 amperes/cm^2. (Magnification of 160X, sample area is 0.690 mm × 0.540 mm)

Figure 14 is of a carbon steel specimen after dissolution in 5N $NaNO_3$ at 1 ampere/cm^2. These are the conditions found to be most favorable for revealing grain structures in copper and INCONEL X-750. As can be seen in the photograph, grain patterns were lacking. What the photograph does reveal is a very thin layer, probably of oxides, on the surface. The dark regions appeared to be the bare metal and the bright regions the oxide. After dissolution into chloride solutions a similar surface was observed.

D. MONEL K-500

MONEL K-500 was chosen because it was essentially a nickel-copper alloy and it was hoped that its anodic behavior could be interpreted, in part, as a function of the behavior of its constituents. It was observed that there were some similarities between the behavior of MONEL and its components, copper and nickel, but this alone did not explain the anodic behavior of the alloy.

The similarities with copper were strongest when dissolution occurred into chlorate solutions, where MONEL showed a very clear voltage transition at low current densities. This voltage transition was smaller than was observed with copper and occurred after dissolution had proceeded for a longer period of time. At high current densities, MONEL appeared to shed layers of solids, but this was not accompanied by periodic voltage oscillations (copper produced oscillations in chlorate solutions at all current densities except the highest, 20 amperes/cm^2). The layers of green fluffy solid reaction products did not possess the cohesiveness observed with copper at low current densities but were very similar to the shedding of solids observed with copper at high current densities. Nickel dissolution under the

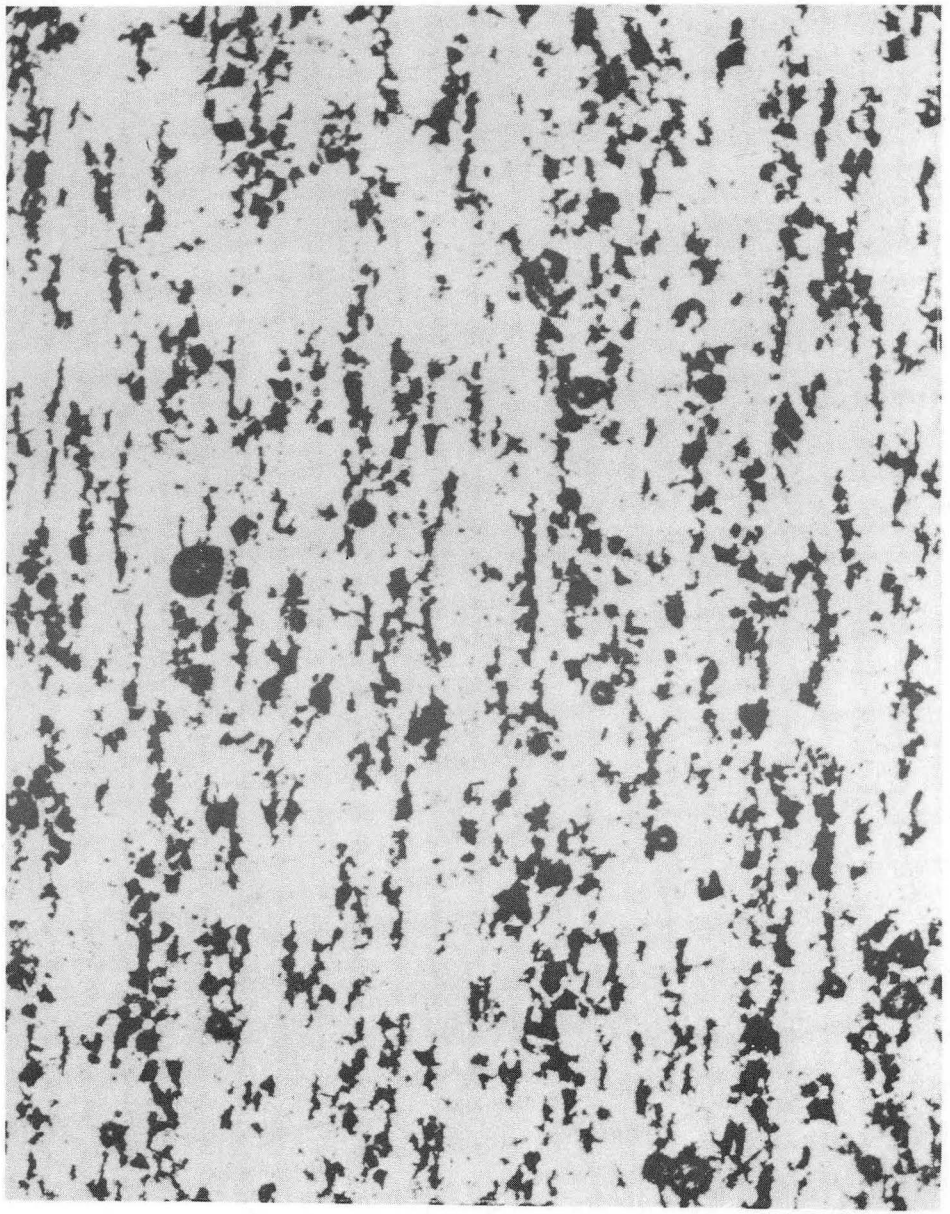

XBB 716-2505

Fig. 14. Carbon steel after dissolution in 5N $NaNO_3$ at 1 ampere/cm^2. (Magnification of 160X, sample area is 0.690 mm × 0.540 mm)

same high current density conditions produced so much gas that any solids produced were not visible.

In the evolution of gas at low current densities, and the lack of a voltage transition in all cases (except chlorate solutions at low current densities), the dissolution of MONEL was similar to that of nickel.

Under some conditions, particularly high current density dissolution into chloride solutions, "pits" were observed on the metal surface. There was no noticeable oxide layer on the surface and the pits had the appearance of randomly distributed shallow depressions, rather than pores or holes.

Figures 15 and 16 are of a MONEL sample after dissolution into a $NaClO_3$ solution at 1 and 20 amperes/cm^2, respectively. What the patterns represent is not known. Nickel and copper are mutually soluble in all proportions, so the alloy should have a single phase. MONEL K-500 contains small amounts of aluminum and titanium, which may form the gamma prime phase; $Ni_3(Al,Ti)$[26]. However, the sample was not age-hardened, in the hope that a single phase could be maintained in the alloy, so no grain boundaries should be present. Samples will generally exhibit only randomly dispersed nonmetallic inclusions, metal sulfides or silicates.[26] The difference in the patterns resulting from high and low current density dissolutions may be due to the greater selectivity of low current density dissolution, if the patterns represent different phases.

E. INCONEL X-750

INCONEL X-750 was the second of the three nickel alloys studied. Its anodic behavior was similar to that of HASTELLOY X, and to a

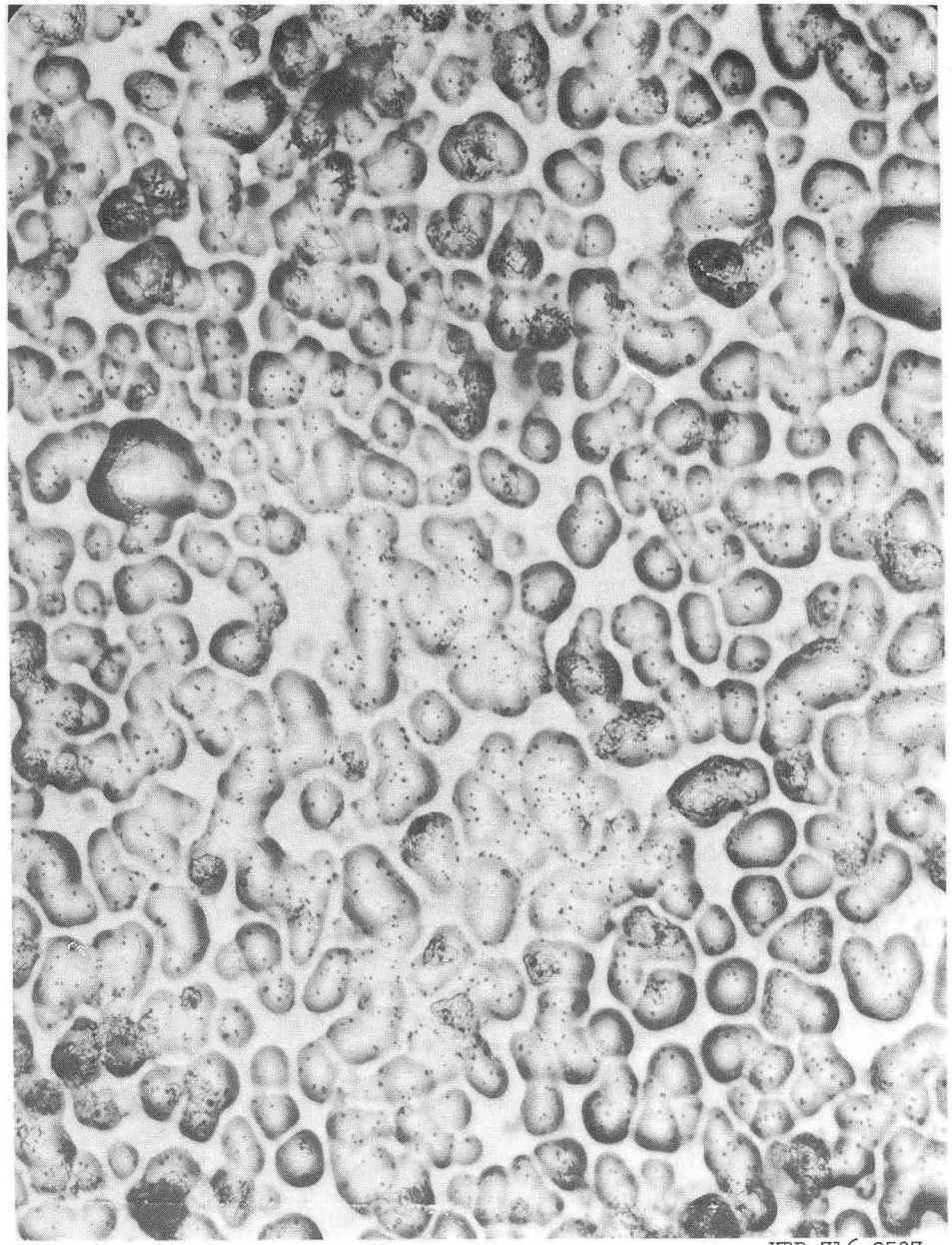

XBB 716-2507

Fig. 15. MONEL K-500 after dissolution in 5N $NaClO_3$ at 1 ampere/cm^2. (Magnification of 400X, sample area is 0.271 mm × 0.212 mm)

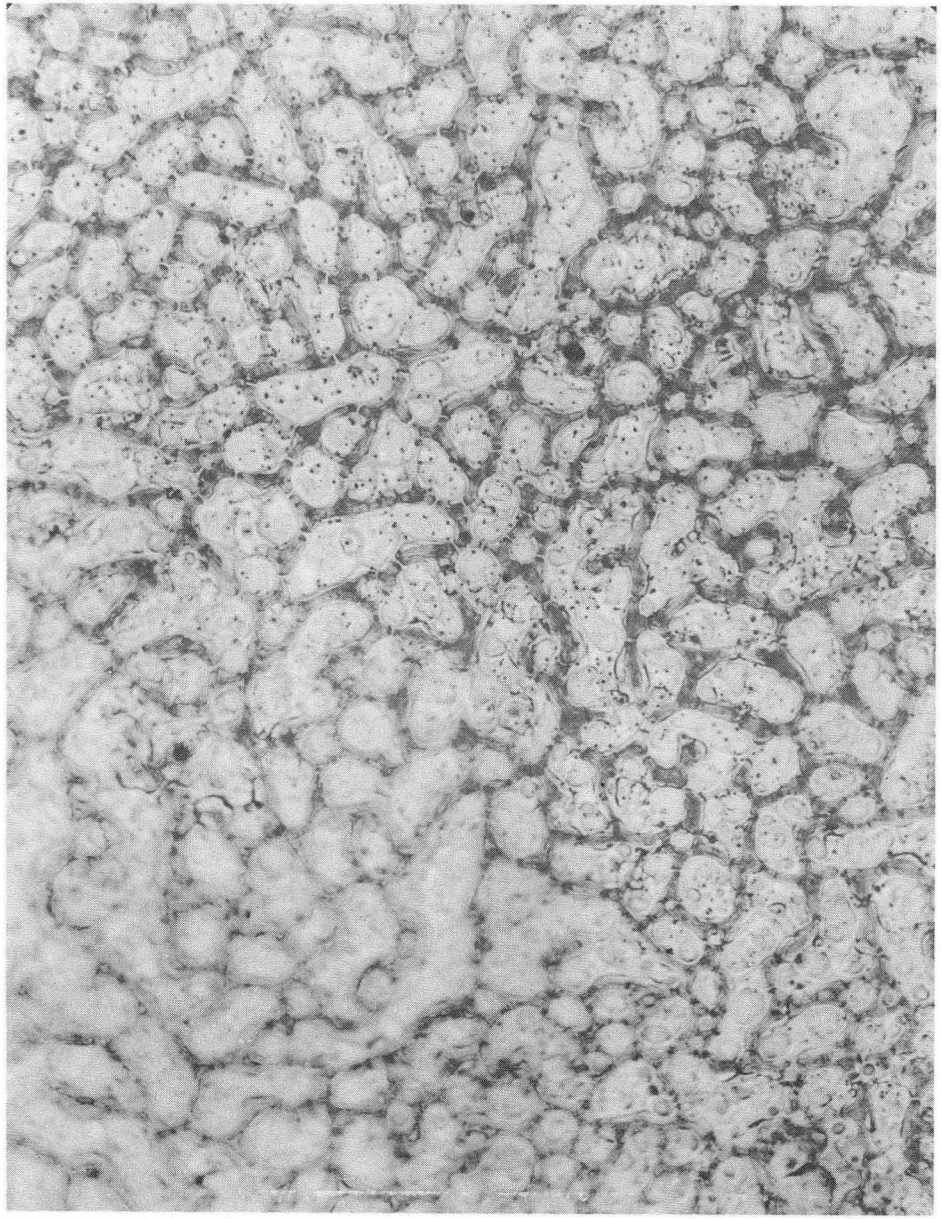

XBB 716-2509

Fig. 16. MONEL K-500 after dissolution in 5N $NaClO_3$ at 20 amperes/cm^2. (Magnification of 400X, sample area is 0.271 mm × 0.212 mm)

lesser degree nickel. There were few similarities with MONEL K-500.

Solid reaction products were clearly evident during high current density dissolution. While dissolving into 5N NaCl, the reaction products were predominantly dark green, finely divided solids. A finely divided black solid reaction product resulted from the dissolution (at 20 amperes/cm^2) into solutions of $NaNO_3$ and $NaClO_3$. At low current densities a yellow gel-like reaction product, similar to that produced with HASTELLOY X, was formed.

The volume of gas evolved was generally moderate. Voltage fluctuations were most pronounced during dissolution into chlorate solutions, and these were on the order of 5 volts. Gas evolution at low current densities was similar to that of nickel; there was no gas evolution with HASTELLOY X.

Figure 17 is representative of the surfaces resulting from the dissolution of INCONEL X-750. This alloy had a definite grain structure, as the result of age-hardening, which was revealed in all the dissolution experiments, but was most detailed after dissolution into nitrate solutions. The grain boundaries were preferentially dissolved as can be seen in the photographs and as was measured by surface profiles. Grain patterns such as these have been reported by Evans and Boden during the electrochemical dissolution of a similar nickel-based alloy, NIMONIC 80A.[34] The figure also shows a fine structure appearing as spots within each grain. These are similar to published photographs which identified similar inclusions as titanium and columbium nitrides.[27] Also apparent is the presence of bands of different shades within grains. Again, these are similar to published photographs of other alloys in which these bands were identified to be

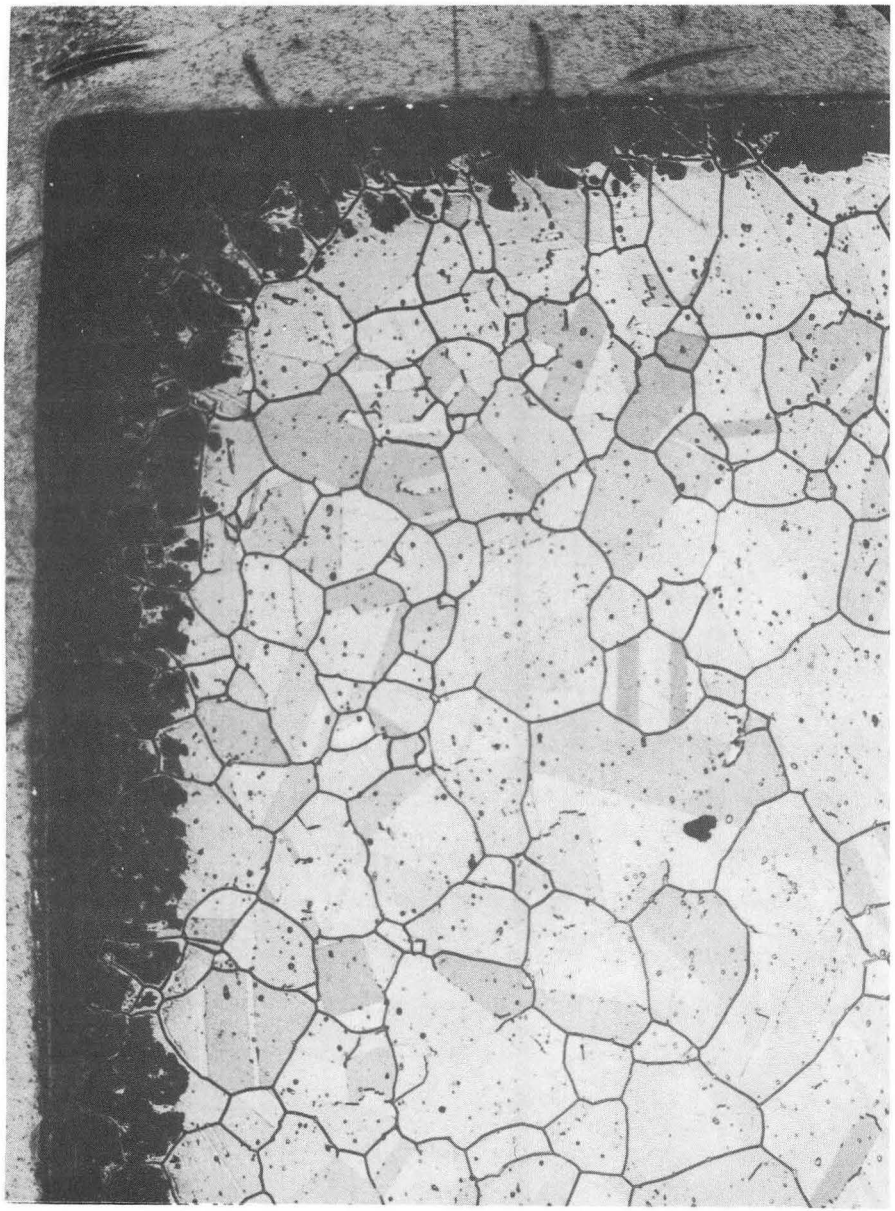

XBB 716-2506

Fig. 17. INCONEL X-750 after dissolution in 5N $NaNO_3$ at 1 ampere/cm^2. The dissolved gap can be seen at the epoxy/metal interface. (Magnification of 40X, sample area is 2.71 mm × 2.12 mm)

the result of twin boundaries.[35]

A gap along the metal/epoxy interface, similar to that shown in the surface profiles for copper (Figure 11), can be seen in the photograph for INCONEL X-750. At high current densities, large shallow pits often developed along the edges of the electrodes.

F. HASTELLOY X

The samples of HASTELLOY X were not characterized as well as the other metal samples in this study; a detailed chemical analysis and careful heat treatment were lacking. Therefore, conclusions drawn from the behavior of this metal are less certain than for other samples investigated.

At low current densities, an iris pattern was observed in all three electrolytes. The iris was composed of what appeared to be the same kind of reaction products, a yellow-brown material that had the appearance of a gel when dissolution occurred in chloride solutions, but was more solid when dissolution occurred in nitrate and chlorate solutions. During low current density dissolution into nitrate solutions, "interference" fringes of different colors, forming at the edges and growing toward the center of the anode like irises, were observed. These probably represent the growth of a thin layer that has a thickness of approximately the wavelength of light.

This was the only metal for which there was no gas evolution, in any electrolyte, at 1 ampere/cm^2. At high current densities there was less gas evolution with HASTELLOY X than with the remaining metals. The reaction products seemed to occupy a thin fluid layer near the

anode, there these products resulted in a darkly colored solution. It was not clear whether the products were solids or a concentrated solution of soluble products. To see if a concentrated solution of metal salts in a thin fluid layer could produce the same effect as was observed during the dissolution of HASTELLOY X, an experiment with a liquid wedge was performed. Two glass slides were clamped at one end and held slightly apart at the opposite end. Into this "glass wedge" samples of saturated solutions of several salts were placed. It was determined that some salt solutions, particularly saturated chromic nitrate (which is black), could produce very dark liquid films. The experiment did not prove the products were soluble saturated salts, but did not deny the possibility. Since molybdenum is used as a primary component, to impart corrosion resistance to the alloy, it may be the cause of differences observed between HASTELLOY X and INCONEL X-750.

The HASTELLOY X surfaces resulting from dissolution were very flat, except near the edges. Figure 18 shows one metal sample. A grain structure and the presence of different solid phases can be seen clearly. The presence of grains is not significant, because even polished surfaces sometimes revealed the same type structure, depending upon the metallurgical history of the sample.

G. Electrolytes

The primary difference among the three electrolytes was observed to be the volume of gas evolved accompanying dissolution. At low current densities, there was no gas evolution in chloride solutions. In nitrate solutions at low current densities, there was no gas evolution accompanying the dissolution of copper and HASTELLOY X, but

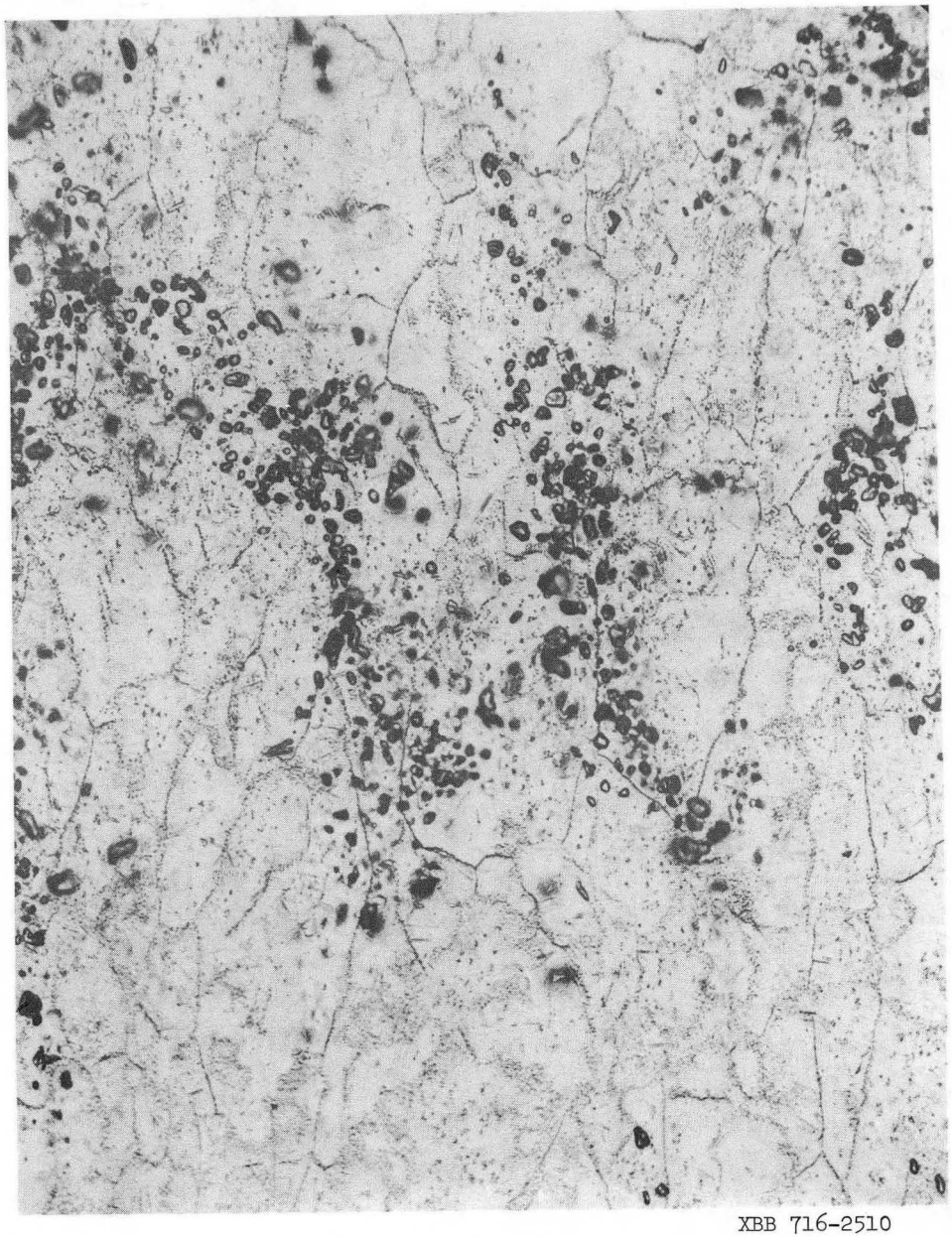

XBB 716-2510

Fig. 18. HASTELLOY X after dissolution in 5N $NaClO_3$ at 20 amperes/cm^2. (Magnification of 160X, sample area is 0.690 mm × 0.540 mm)

small amounts of gas were produced during dissolution of the remaining metals. Only the dissolution of HASTELLOY X was not accompanied by gas evolution when the metals were dissolved into chlorate solutions.

At high current densities, the volume of gas was clearly smallest in chloride solutions and greatest in chlorate solutions. With chlorate solutions, and to a smaller extent with nitrate solutions, there were fluctuations of the cell voltage that seemed to be related to the gas bubbles on the anode surface. Gas bubbles sometimes coalesced into one large bubble, effectively insulating the anode from the electrolyte. An increase in cell voltage, beyond the limits of the power supply, was observed to accompany the formation of these gas layers. When smaller voltage fluctuations were measured in systems where large amounts of gas were produced, it was assumed that the gas again insulated the surface, but less effectively than in cases where the voltage fluctuations were very large. Large voltage fluctuations were most pronounced during the dissolution of nickel and carbon steel. When the voltage fluctuations were small, there was no clear correlation between the presence of fluctuations and any visible feature of the evolved gas, for example, bubble size and distribution of bubbles over the surface of the anode.

It was possible to observe one of the cathodes during the dissolution experiments. In nitrate solutions, the volume of cathodic gas was significantly smaller, especially at low current densities, than during experiments in chlorate solutions. This was probably due to the reduction of nitrate ions in solution.

There were differences in the quantity of solids produced by metal dissolution in the different electrolytes. Generally, there

were fewer solids in chloride solutions than in nitrate or chlorate solutions, probably due to the ability of chloride ions to form soluble chloride complexes with most of the metals studied here. However, the quantity of solids was more strongly a function of the metal dissolved than of the electrolyte into which the metals were dissolved. For example, copper produced large quantities of solids while dissolving in all electrolytes; the quantity of which increased in the order: chloride, nitrate, and chlorate. HASTELLOY X dissolution produced the smallest amount of solids in the same electrolytes.

The surface finishes resulting from dissolution of the electrodes also differed among the three electrolytes. Chloride solutions generally resulted in pitted or "corroded" surfaces. Nitrate solutions produced etching conditions, particularly at low current densities. The grain structure of copper and INCONEL X-750 was revealed best by dissolution in nitrate solutions at low current densities. After dissolution in chlorate solutions, the surfaces were generally smooth. Polishing conditions, over a significant portion of the metal surface were not observed under anv of the conditions studied here. There was some polishing along the edges of most of the electrodes dissolved at high current densities. However, these areas were never flat or extensive.

V. DISCUSSION

Whereas the results were primarily observations grouped according to the metal or electrolyte studied, this section will attempt to relate those observations to the three questions (mentioned in Section I.B. Scope) that this study sought to answer: the relationship between the observed phenomena and cell voltages, the generality of solid and gaseous reaction products with different metals, and the occurrence of periodicities. Unfortunately, the phenomena observed in this study were so complex and intertwined that they could not be conveniently grouped into separate sections. Therefore, it will often be necessary to refer back and forth among the sections in order to support an idea being developed. First, a few comments are made on the current density distribution and hydrodynamic conditions encountered with this particular experimental apparatus.

A. Current Distribution and Hydrodynamic Conditions

In this study, it was not possible to use the traditional parallel plate electrode configuration previously used by most researchers. The cathodes were placed at right angles to the anode so observations of the anode surface could be made (see Section II. Experimental apparatus and procedure). Therefore, it seems appropriate to begin the discussion of results with a few comments on the current distribution and hydrodynamic conditions under which the experiments were performed.

Current distribution

Due to the complex cell geometry, and unknown overpotentials, no attempt was made to predict the current density distribution on

the anode surface in advance. In any event, this distribution would be expected to change as the metal dissolved, since the electrode receded below the epoxy in which it was cast. The most accurate method of evaluating the current density distribution seemed to be by surface profiles of the dissolved electrodes. Figures 11A and B are profiles of a copper electrode after dissolution. The profiles show sharp gaps at the metal/epoxy interface, but otherwise the surface appears to be fairly flat. With the remaining alloys, the dissolution at the edges was greater than with copper, but the central electrode regions were generally smooth. From microscopic observations of a large number of electrodes, it appeared that the electrodes were uniformly dissolved, except for the gaps at the edges.

A satisfactory explanation for the separation at the juncture between the epoxy and metal has not been obtained. One conjecture was that the metal electrodes heated during dissolution and expanded. The epoxy was assumed to be permanently deformed by the anode expansion, so that upon cooling after the experiment, a narrow gap resulted. However, examination of the gaps under a microscope revealed pits and ridges along the sloped sides of the metal. Thus, it appears that the electrodes were dissolved and the conjecture that the gap was due to the expansion of the metal was not supported by the observations.

A study of the motion picture films for the dissolution events at 20 amperes/cm^2 revealed a number of cases where gas evolved at the anode surface in a horseshoe pattern with the opening of the "horseshoe" facing upstream. If the evolved gas is assumed to be steam, this would indicate a higher current density in the gas

producing regions than in the non-gas producing regions. This follows from the assumption that steam would be produced by power dissipation, given by I^2R, in a thin layer at the anode surface. It is assumed that R, the resistance across the layer, is the same for all points on the anode and that differences in the flow velocity, across the width of the channel, would not dissipate heat more rapidly from one region than another. Both assumptions appear reasonable if the layer is considered to be either a laminar fluid layer or a layer of solid products. Assuming that the chemical reactions are the same everywhere on the anode surface, a higher current density would produce more extensive dissolution. Therefore, if the evolved gas in a "horseshoe" pattern is assumed to be steam, then dissolution should be more extensive in the region of the "horseshoe". However, the electrodes appeared to be fairly flat. In Section D. Evolution of gas, it will be shown that the Faradaic efficiency was less than 100 percent for the metal dissolution reactions. From these facts, it is concluded that the local current density, at 20 amperes/cm^2, was highest along the edges of the anode closest to the cathodes and that the current density in excess of that found in the center of the electrode produced oxygen. This conclusion results in the observation that different chemical reactions occurred at the anode surface, a surface that should have the same potential throughout, when the current density was higher in one area than another.

Hydrodynamic conditions

There were two aspects to this topic: (1) to assure that there was a fully developed, undisturbed, velocity profile at the electrodes by using an adequate entry length and by accurately positioning the

anode, and (2) to determine the effectiveness of mass transfer correlations to predict the active/transpassive transition, or more generally, the active/transpassive regions of dissolution when the transition was not clearly defined.

The entrance length of 70 hydraulic diameters assured the presence of a fully developed flow, whether laminar or turbulent, in the electrode region.[36,37] The anode surface was not precisely parallel to the channel bottom, due to a slight misalignment of the axis of the electrode perpendicular to the flow channel. Therefore, one edge of the epoxy, in which the electrode was cast, was flush with the channel while the other edge was 50-100 microns below the channel surface. At high current densities, the electrodes receded about 50-100 microns, during one experiment, as they dissolved. Since the hydraulic diameter was 7.5 mm, the sum of the errors resulting from positioning and dissolving the anode was less than 3 percent of the hydraulic diameter.

One theory, proposed to explain the transition from an active to a transpassive mode of dissolution, supposes that the transition occurs when the rate of dissolution exceeds the mass transfer limits for the dissolution products in the mass transfer boundary layer. Rapid dissolution might result in salt crystallizing out on the electrode. This theory was used in selecting parameters for the experiments, so metals could be studied in both the active and transpassive regions. The correlations are given here, following the procedure of Landolt, et. al.[17]

Landolt reported a formula for the Nusselt number as follows:

$$Nu = \frac{i\ D_h}{2\ F\ c_s\ D} \qquad (1)$$

where

i = current density, amperes/cm^2

D_h = hydraulic diameter; 0.75 cm for the channel used in this study

F = Faraday's constant, 96,500 coulombs/g-equiv.

c_s = saturation concentration of the dissolving species, g-equiv./cm^3

D = diffusivity of the dissolving species, cm^2/sec

In most cases enountered in this study, order of magnitude figures for the physical properties were used: $c_s = 5 \times 10^{-3}$ g-equiv./cm^3 and $D = 10^{-5}$ cm^2/sec. With these figures, the Nusselt number is given by:

$$Nu \cong 75\ i \qquad (2)$$

The Reynolds number is given by:

$$Re = \frac{u\ D_h}{\nu} \qquad (3)$$

where

u = the linear flow velocity, cm/sec

ν = the kinematic viscosity, cm^2/sec

If $\nu \cong 10^{-2}$ cm/sec, the Reynolds number is given by the following equation:

$$Re \cong 75\ u \qquad (4)$$

The correlation for Nu versus Re in fully developed laminar flow is given by:[38]

$$Nu = 1.85\ (Re\ Sc\ D_h/L)^{1/3} \qquad (5)$$

where

Sc = Schmidt number; ν/D

L = distance from the leading edge of the electrode; here taken to be the electrode length of 5 mm.

For fully developed turbulent flow in the mass transfer entrance region, the equation as given by Van Shaw, Reiss and Hanratty is:[39]

$$Nu = 0.28\ Re^{0.58}\ (Sc\ D_h/L)^{1/3} \qquad (6)$$

The six metals used in this study were dissolved in three electrolytes at 1 and 20 amperes/cm^2 and electrolyte flow velocity of 10 cm/sec. Using equation (2) and the current densities of 1 and 20 amperes/cm^2, the corresponding Nusselt numbers are 75 and 1500 respectively. Using equation (4) and the electrolyte flow velocity of 10 cm/sec, the Reynolds number for the experiments was computed to be about 750. If mass transfer considerations alone determine the point at which the active/transpassive transition occurs, and the correlations are valid, the Nusselt number corresponding to the transition point (Nu_t) can be found using equations (5) or (6). For the case of Re = 750, equation (5) gives a computed value of $Nu_t = 400$ as the mass transfer limit in fully developed laminar flow. This means that experiments conducted for $Nu < 400$ should be below the mass transfer limits, and hence, would be in the active dissolution

region. For Nu > 400, the experiments would be in the transpassive region. The actual value of the Nusselt number for a given experiment, as given by Equation (2), is a function only of the current density. By setting the current density at 1 ampere/cm^2, Nu = 75, which is less than the transition value of 400. Thus, the experiment was predicted to be in the active dissolution region. Similarly, selecting a value for the current density equal to 20 amperes/cm^2 would result in transpassive dissolution.

There are two difficulties with the analysis presented above. First, the idea of a mass transfer limit as the determining factor in the active/transpassive transition is plausible, but it has not been proven. Second, the identity of the dissolving species and its physical properties, needed to evaluate Equation (1), are not well known; estimated values must suffice with the possibility of large errors.

B. Voltage Phenomena

The first objective of this study, as indicated in the Scope, was to determine the relationship between the visually observed phenomena and the measured cell voltages. This section begins with a comparison of the computed and observed cell voltages, then a discussion of the active/transpassive transition voltages will be given, and finally the effect of gas bubbles on cell voltages will be noted.

Cell voltages

The ohmic resistance of the electrochemical cell could not be calculated by any convenient method because of its complex geometry. For this reason, the cell constant (L/A) for the flow channel was

computed from the cell resistance, measured using a precision a.c. bridge, and the resistivity of a standard electrolyte. (The resistance was measured to be 92 ohms at 20 kilohertz in a 0.1N NaCl solution with a resistivity of 93.7 ohm-cm. The anode was made of polished nickel and the cathodes were of stainless steel.) The value of the cell constant was calculated to be 1.0 cm^{-1}. For the 5N electrolytes used in this study, the molar conductances were about 50 $ohm^{-1}cm^2$/mole. From this the computed resistivity was about 4 ohm-cm. Hence, with 5N solutions the cell resistance is calculated to be about 4 ohms.

The cell resistance is composed of an ohmic electrolyte resistance and "resistances" at the anode and cathode surfaces due to the charge transfer reactions. The ohmic resistance is a linear function of the current density and is directly proportional to the cell constant.* The surface overpotentials probably obey the Tafel relationship; they increase approximately logarithmically with the current density.[18]

For low current density dissolution, at 1 ampere/cm^2 (total current of 0.25 ampere) the predicted ohmic drop is 1.0V. The average observed cell voltages, found by summing the observed cell voltages for all the metals in one electrolyte (data in Table VIII) and dividing by the number of observations, are given below.

---

* The current distribution, and hence the cell constant, is different at finite d.c. currents from the one obtained by the one obtained by the a.c. bridge technique. Nevertheless, the use of the a.c. cell constant for the d.c. applications represents a good approximation.

Electrolyte	Average voltage
NaCl	2.9[a]
$NaNO_3$	3.5
$NaClO_3$	4.2[b]

a. Average does not include the value for copper, which was much higher than for the other metals.

b. Average uses a value of 4.0V for MONEL K-500.

According to these figures, a voltage drop of 2-3V should be ascribed to the sum of the electrode potentials. The measured voltages were higher than the estimated voltages because of the anodic and cathodic electrode potentials, which include thermodynamic and kinetic components. The measured voltage drop increases with the sequence of electrolytes: chloride, nitrate and chlorate. This sequence of electrolytes is also the same as that for increasing volumes of gas evolved. The high voltage value for copper dissolution into chloride solutions is probably explained by an oxide layer on the surface, since no gas evolution was observed.

At high current densities, 20 amperes/cm^2, the predicted voltage drop across the cell was 20V. Excluding the extreme values for nickel and carbon steel dissolving into chlorate solutions, which seem to be due to gas blanketing the entire anode surface, the average voltage drop (computed as mentioned above) was the same for each electrolyte; 25V. The 5V average difference is not unreasonable if one considers the larger overpotentials and larger gas volumes at the higher current densities.

Active/transpassive voltage transition

The occurrence of a voltage difference between dissolution in the active and transpassive modes is well known.[40] Correlations of visual observations and voltage phenomena have been made (e.g., Pigeaud and Kirkpatrick's potentiostatic microscopic study of iron passivation in sulfuric acid[41]). However, this study is believed to be the first to attempt a direct correlation of visual observations and cell voltage measurements for high current density events.

In this study, the most clearly defined transition voltages occurred with copper in free convection; see tabulated voltages in Section IV.A.1. Free convection. The cell voltages show a definite correlation with the "iris" patterns. During the active introduction period to the transpassive dissolution, the solid layer of reaction products grew from the edge of the electrode toward the center and the voltage remained constant at a low value (5-10 volts). When the iris closed up at the center, the voltage rose to a high value (20-40 volts). During the transpassive, high-voltage dissolution, solid reaction products were produced uniformly across the entire surface. For the copper/chlorate system, the reaction appeared to oscillate between the high and low voltage regions, that is, between the transpassive and active modes of dissolution. Visually, the rise of the cell voltage coincided with the growth of the last of three irises and the drop in cell voltage coincided with the shedding of a solid layer of reaction products (see tabulated results in Section IV.A.2. Forced convection).

In forced convection, at low current densities, copper showed the same type voltage transition it had shown in free convection.

However, carbon steel, nickel, and most of the nickel base alloys showed no active/transpassive voltage transition. The only exception among the nickel base alloys was MONEL K-500 which showed a gradual inflection in its voltage curve when dissolving in 5N $NaClO_3$.

At high current densities, a very rapid formation of irises was observed for copper, but the pen recorder response was not rapid enough to record the voltage transition curve.

As mentioned in the previous section, where the active and transpassive regions were predicted from mass transfer correlations, all the low current density experiments were expected to be in the active region and the high current density experiments in the transpassive region. For the transpassive region, the prediction appeared to be valid. In fact, copper/chlorate, which normally oscillates between the active and transpassive modes, remained in the transpassive and showed no signs of oscillations. For the active region, copper started dissolving at a low voltage and jumped to the higher voltage mode in less than a half second. With all the metals, solid reaction products formed under conditions that were predicted to yield soluble reaction products. The length of the experiments was limited by the camera spring drive (see Section II.B. The optical system). Therefore, the possibility that a solid layer might form, requiring a much longer time span than copper, after which the voltage remained at a low value and the metal dissolved as a soluble species by diffusing through the layer was not explored. This would reconcile the observations of fairly low cell voltages with the production of solid reaction products.

Gas bubble effects

From Table V, for gas evolution observed during high current density dissolution, it can be seen that two thirds of the dissolution events produced some form of voltage fluctuations and that half of the events produced voltage fluctuations greater than 2 volts. When correlated with the estimated gas evolution volume, all those systems observed evolving large volumes of gas produced fluctuations; normally large fluctuations. The general results are obvious; large amounts of gas evolved produced fluctuations in the cell voltage.

The effect of gas bubbles on the cell voltage was most dramatic when nickel and carbon steel were dissolved into chlorate solutions. Gas covered the entire surface and would periodically coalesce into one large bubble, that was subsequently swept off the surface. When the surface was covered by one of these large bubbles, the voltage would exceed the upper limit of the power supply. Of the remaining cases of gas evolution, about half evolved in the shape of a "horseshoe" with the open end facing upstream and half evolved as a layer of bubbles of uniform size packed in a single layer over the entire surface. No correlation could be found between the small voltage fluctuations and either pattern of gas evolution.

During the dissolution of copper in stagnant solutions, gas bubbles adhered to the junction between the insulating varnish and the copper electrode, creating a "halo" of bubbles. With experiments conducted in the flow channel, a behavior similar to this was observed. However, in most of the experiments the gas was observed to evolve on the anode surface, so it seems unlikely that the nucleation sites provided by the epoxy/metal interface were a significant factor in the

pattern.

C. Formation of Solids

In this section a number of topics related to the nature of the solid reaction products produced during anodic dissolution will be considered: conditions in which solid reaction products were observed, pores in solid films on copper, etching and pitting in alloys, and the possible role of photoelectrochemical effects.

Solids

Determining the presence or absence of solid reaction products during high current density dissolution was a primary objective of this study. This qualitative observation should provide much information on the chemistry of the reaction products and the mechanism of transport of the products from the anode surface. The presence or absence of observed solid reaction products is indicated in Table IX.

With some of the metal/electrolyte combinations, a definite conclusion as to the presence of solid reaction products was hindered by the volume of gas evolved. This was the case with nickel and carbon steel, in particular. A second difficulty was that of distinguishing between a very finely divided solid product and a concentrated solution of metal salts. In many cases, a highly colored solution resulted at the anode surface from dissolution of the metal.

For the dissolution of copper in free and forced convection, solid reaction products were almost universally observed at all current densities and in all electrolytes. The one exception was in chloride solutions at low current densities (3 amperes/cm^2), where soluble

Table IX. Were solid reaction products observed during anodic dissolution?

Metal	Electrolyte					
	NaCl		$NaNO_3$		$NaClO_3$	
	1 A/cm^2	20 A/cm^2	1 A/cm^2	20 A/cm^2	1 A/cm^2	20 A/cm^2
Copper	yes[a]	yes[d]	yes	yes	yes	yes
Nickel	no[b]	yes	?[e]	?[f]	yes	?[e]
Carbon steel	no[b]	yes[d]	?[e]	?[g]	yes[h]	?[e]
MONEL K-500	no[b]	yes	?[e]	yes	yes	yes
INCONEL X-750	no[b]	yes	yes	yes	?[e]	yes
HASTELLOY X	yes[c]	yes[d]	yes	yes[d]	yes	yes[d]

References to Table IX

a. At this current density solids oozed through pores in a layer of solid reaction products covering the anode surface. In stagnant solutions at 3 amperes/cm^2, the reaction products were soluble copper chloride complexes.

b. No solid products were observed being swept off the anode surface, although there was a layer of solids produced on the surface. This layer formed during the first few second of dissolution and showed no change during the last few seconds of dissolution.

c. The reaction product was gelatinous.

d. The appearance was that of a concentrated salt solution of the metal ions in which solid products were often not clearly identifiable.

e. Gas evolution obscured any reaction product, whether solids or dissolved species.

f. Some solid were observed along the anode edges, but gas evolution obscured the center of the electrode. After dissolution the surface was observed to be etched.

g. Dissolution at the edges of the anode. The dissolved surface had a resemblance to a sand blasted surface.

h. The edges were dissolved, but there was no sign that the center had been dissolved; scratches from polishing were still clearly visible.

copper complexes seemed to be the only reaction product. But even in this case, where the continuously produced reaction product was soluble, the anode was initially covered by a layer of solid reaction products.

The "iris effect" (first mentioned in Section V.A.1. Copper, free convection), was an important indication of the presence of solid reaction products. While at low current densities it was not possible to determine whether or not solid reaction products were being continuously produced, the iris effect at the very least indicated the formation of an initial layer on the anode surface. Presumably this layer was often an oxide or a hydroxide, although no chemical tests were performed to determine this. No metal produced as dramatic or as clearly defined an iris as did copper. In contrast, a few of the metals, especially at high current densities, did not reveal any iris pattern at all.

Pores

As mentioned in the results, when high purity copper (ASARCO, 99.999) was dissolved into nitrate solutions, over a wide range of current densities, a pattern of pores and grains appeared; see Figs. 9 and 10. These pores and grains extended in depth through the oxide layer into the dissolving copper metal. No other metal studied here revealed any form of pore structure, although grain patterns appeared when some metals were dissolved, as will be noted in the next section on etching. When copper dissolved into chloride solutions, it showed the puzzling ability to dissolve as a soluble copper complex, insoluble solids, or solids with evolving gas, depending upon the current density. At low current densities (1 ampere/cm^2), the solid reaction

products oozed through pores in a layer of solid reaction products covering the anode surface. Only the behavior of copper dissolving into nitrate solutions will be considered here.

Figures 9 and 10 reveal two overlapping grain structures and a pattern of pores. One grain of the large grain structure, with grains on the order of 1 mm in diameter, is represented by the dark area to the left of the center in the photographs. The small grain structure shows clearly in the photograph as a pattern of polygons, normally irregular hexagons, with diameters on the order of 200-300 microns. The pores, spaced about 30 microns from center to center, were often in a hexagonal pattern with respect ot their nearest neighbors, and did not grow on the small grain boundaries, although they did grow on the larger grain boundaries.

The pattern of pores and grains is tentatively explained by a combination of selective dissolution of grain boundaries and the presence of a compact oxide layer. The large grain boundaries are probably old grain boundaries, although they may result from cracks in the oxide layer. The small grain boundaries appear to be new grain boundaries resulting from the recrystallization of high purity copper.[42] Under selective conditions, when the dissolution of a copper surface occurs, the grain boundaries are selectively dissolved.[43] The resulting copper oxide layer appeared to be compact (dense) and to adhere to the copper surface. Reaction products produced by the dissolution probably escaped from the surface through the pores in the oxide layer. These pores do not grow along the new grain boundaries, probably because these boundaries are producing reaction products, just as the pores are. How a point of dissolution shields itself

from encroachment by a neighboring point of dissolution is not known. The pores often cross, or grow on, the old grain boundaries. These boundaries are not dissolved as extensively as the new boundaries of the pores.

The pores are probably not related to the crystallographic nature of the copper sample. The selective dissolution of dislocations and impurities, as reported in the literature, results in a pattern quite different from the pores observed here, although they cover the surface with about the same density.[44-46] The occurrence of grains and sub-grains is common in etches of high purity copper.[47] It was first thought that the large grain structure represented the principal grains and the small grain structure the sub-grains. However, the small so-called sub-grains can be seen in the figures to grow across principal grains. Therefore, the patterns overlap rather than enclose one within another. Thus, an explanation of the occurrence of pores or grains based on crystallographic considerations alone appears to be untenable.

Etching and pitting

Etching was clearly observed with those metals having a definite grain structure, primarily copper and INCONEL X-750. Although these metals revealed etched surfaces after dissolution in all three salt solutions, nitrate solutions were most effective in revealing details in the etched surfaces. Low current densities were more effective in bringing out details than high current densities.

The etching of copper has been mentioned already, in relation to the pores observed in the oxide layer on the copper surface after dissolution. The grain structure of INCONEL X-750 is illustrated

in Figure 17. The grain boundaries show clearly as well as inclusions of titanium and columbium nitrides within the grains. The photograph also reveals parallel-sided regions within the grains. These appear to be twin boundaries (a surface imperfection separating two regions of a crystal which are mirror images of each other with respect to the plane of the boundary).[34] In any case, it seems clear that low current dissolution (1 ampere/cm^2) in nitrate solutions produces very selective dissolution of the metal at regions of impurities and/or dislocations.

Etching was observed on nickel and carbon steel anodes under some conditions. However, the grain size was small (of the order of tens of microns) and could not be compared with the patterns observed with copper and INCONEL.

A randomly distributed pattern of pits was observed on MONEL, as mentioned in the results. With nickel-based alloys at high current densities, pitting occurred along the edges of the electrode.

In chloride solutions, especially at high current densities, "corroding" occurred. This refers to an irregular pattern of extensively dissolved and undissolved areas over the entire anode surface. In stagnant solutions with copper, this occurred mostly along the electrode edges. Since the presence of a solid reaction product was manifestly least in chloride solutions, this pattern of dissolution may be related to the absence of an oxide layer.

Photoelectrochemical effect

It is well known that the behavior of a metal may be altered by bombarding the surface with photons (the photoelectric effect). Barton and Garrison have studied the effect of illumination on the behavior

of the copper/cuprous oxide system and have demonstrated the presence of a photoelectrochemical effect.[48,49] The presence of an oxide layer on the metal surface may greatly complicate the effect, since oxide layers often have semi-conductor properties. During the dissolution experiments performed in this study, the anode surface was strongly illuminated. Therefore, a brief note on how the photoelectrochemical effect might alter the results seems to be in order.

Most research on photoelectrochemical effects has been done at very low current densities, such as Grechukhina and Valeev's study on the mechanism of the anodic dissolution of copper in phosphoric acid using a pulsed light source.[50] Recent work by Kruger and Calvert with copper/cuprous oxide has shown that light results in a limiting oxide thickness on the copper surface when oxidized in oxygenated water.[51] They wrote, "The behavior observed was explained on the basis of a competition between growth and dissolution reactions, the dissolution reaction being promoted by illumination." Neglecting reflections of the light from the fiber light source off the channel cover and adsorption of the light by the electrolyte, the electrode was computed to be illuminated by approximately 0.1 watt/cm^2 during this study. This is considerably higher than the minimum value of 290 microwatts/cm^2 used by Kruger and Calvert. What effect the high level of illumination used in systems with high current density dissolution might have is not know. Extrapolating the results reported in the literature, the oxide layer might be thinner due to the high

level of illumination, and hence lower the voltage drop near the anode surface, but this could not be determined here. As far as could be determined, the results of the high current density experiments conducted in this study are consistent with those conducted by Kinoshita, Landolt, Cooper, and Jacquot on systems that were not illuminated.[14-20,33,52]

D. Evolution of Gas

The problem of anodic gas evolution is central to the understanding of high current density processes. Without an adequate evaluation of the absence or presence of gas, its composition, and its rate of evolution, the composition of the reaction products (particularly the apparent valence of the dissolved metal) will be uncertain. It also seems likely that the turbulence created by rapid gas evolution (analogous to boiling) is an important process in the removal of reaction products from the anode surface. (See also Section V.B. Voltage phenomena, gas bubble effects.)

In studying copper in free convection and at current densities near 3 amperes/cm^2, the evolution of gas was small. It was estimated that the gas evolution, if oxygen, corresponded to about 0.1 - 1 percent of the total current. Such low gas evolution rates could be produced by several different mechanisms. Some of these alternatives will be reviewed here, although experiments with copper and other metals support the view that oxygen is the primary constituent of the evolved gas.

Two possible sources for the anodic gas are: thermal production of steam, or water vapor, or degassing of the electrolyte, due to the ohmic power dissipation in a surface layer, and chemical and/or electrochemical oxidation of the electrolyte to gaseous oxygen. The

electrochemical effects should be proportional to the current and the thermal effects should be proportional to the square of the current.

Thermal effects

Royer[53] has reported observing local boiling when copper was dissolved in 0.91 mole percent sodium chloride solution (bulk temperature, 25°C) at 0.20 amperes/cm^2. Observations in both free and forced convection at current densities up to 4 amperes/cm^2 do not support this observation. In free convection, the bubbles remained stable in size for several minutes after dissolution ceased, with no signs of the gas condensing, as would be expected with steam. In forced convection, bubbles retained approximately the same size when they were swept into the bulk of the electrolyte. A gas bubble would be expected to be stable if the bubble condensed by gaseous diffusion into the electrolyte, because the concentration gradient is normally small, or non-existent, as in solutions saturated with gas. However, a hot gas bubble (100°C) swept into a cold electrolyte (25°C) would be expected to show some change in size.

At current densities higher than several amperes/cm^2 and at low flow rates (i.e., 20 amperes/cm^2 and 10 cm/sec) the possibility of steam evolution becomes significant. About 150 watts were dissipated under these conditions (total current of 5 amperes and voltage drop of 30 volts); this corresponded to 35 calories/sec. At a flow velocity of 10 cm/sec, and with a channel cross sectional area of 0.6 cm^2, the volume of electrolyte adsorbing this heat was 6 cm^3/sec. If the solution was fully mixed, this would correspond to a 6°C temperature rise. However, since the electrolyte was in laminar flow (Re = 550) when it arrived at the anode, and since the current density

was probably higher near the anode edges closest to the cathodes, it is conceivable that the power dissipation in a fluid layer near these edges was much greater than that computed above. The assumption of pure laminar flow was not entirely correct, since some mixing was produced by gas evolution in all the high current density experiments. Even if the electrolyte did not boil, the evolving gas could be assumed to be saturated with water vapor. As shown in the table below, the volume of water vapor in the gas evolved could be substantial at electrolyte temperatures well below boiling.

T, °C	Vapor pressure of water[a] mm Hg	Percent of total pressure
25.0	23.756	3
46.1	76.04	10
65.0	187.54	25
82.0	384.9	50
92.1	569.12	75
100.0	760.00	100

a. Chemical Engineers' Handbook, edited by John H. Perry

Another possible explanation, in terms of thermal effects, is degassing of the electrolyte. For a current density of 3.15 amperes/cm^2 (total current of 1 ampere and an anode surface area of 0.317 cm^3) and 30 volts, the power dissipation is 30 watts (or 95 watts/cm^2). If half of this power is assumed to be dissipated in the anode region, and is used to heat 1 cm^3 of stagnant solution (whose properties are assumed to be those of pure water), the liquid temperature will rise from 25°C to 28.5°C in one second. The solubility of air in water is inversely proportional to the temperature and may be computed using

Henry's law. The Henry's law constant is approximately a linear function of temperature. Therefore, the volume of the electrolyte assumed to be degassed will not alter the calculations significantly, as long as the electrolyte temperature is below boiling (i.e., as much gas is released from a small volume heated greatly as from a large volume moderately). Assuming that 1 cm^3 of electrolyte was saturated with air before and after dissolution, the heating would produce an evolution of air of approximately 8×10^{-4} cm^3/sec. This corresponds to about 200 bubbles with diameters of 0.2 mm (compared with observed 10 - 20 bubbles of diameter 0.1 to 0.5 mm; gas evolution of 10^{-4} to 10^{-5} cm^3/sec). The calculations have been explained carefully so the assumptions upon which this explanation for the evolution of gas rests will be evident. Qualitatively, the observed gas evolution for copper dissolution at low current densities in free convection could be due to degassing of the electrolyte.

Oxygen evolution

Kinoshita has reported, for copper dissolving into solutions of KCl, KNO_3, and K_2SO_4 at current densities up to 80 amperes/cm^2 and in a specially constructed flow system, that if oxygen was produced during anodic dissolution, it corresponded to evolution by less than 1 percent of the applied current.[16] He did not succeed in measuring the actual oxygen concentration, but concluded that his apparatus could measure oxygen produced by more than 1 percent of the total current. Using this value of 1 percent, with the free convection experiments considered here, 6×10^{-4} cm^3/sec of oxygen would be produced. In the present study, gas was observed and was estimated

to be evolved at a rate with this order of magnitude; i.e., the rate of gas evolution observed here could probably not have been measured by Kinoshita's methods.

Kinoshita, et.al., have also reported that copper dissolved in the transpassive mode with an apparent valence of 1.5 - 1.6 (this assumed no oxygen was evolved).[15] Calculations, to be explained below, for copper dissolving at 40 amperes/cm^2 (2N KNO_3, electrolyte flow of 150 cm/sec), showed close to 100 percent current efficiency if the copper was assumed to dissolve to copper (II); an apparent valence of 2.

In this study it was not possible to collect gas samples or perform weight loss measurements because the amount of dissolution was small; normally about 10 microns of surface was dissolved, and never more than 200 microns. For copper at the maximum dissolution depth, the weight loss would be about 0.05 percent of the total weight of the electrode. The restriction on the depth of dissolution was necessitated by the desire to maintain a reasonably well defined cell geometry. However, starting with polished samples and measuring the depth of dissolution, the volume of metal removed was determined. The equivalents of metal dissolved, assuming a valence, was then computed. The total charge passed could be determined from plots of current versus time. The ratio of the equivalents of metal dissolved to the charge passed (times Faraday's constant) was defined to be the current efficiency. This procedure could only be used for extensively dissolved electrodes which also had well defined surface profiles. Thus, this method was used for determining the current efficiencies for nickel, carbon steel (both at 20 amperes/cm^2 and electrolyte flow of 10 cm/sec),

and copper (40 amperes/cm^2 and electrolyte flow of 150 cm/sec). No attempt was made to determine current efficiencies for the alloys studied, since the large number of possible reactions constitute a very complex chemical system. The table below lists the current efficiencies computed.

Current efficiencies by volume loss method

Metal	Electrolyte			Reaction
	NaCl	$NaNO_3$	$NaClO_3$	
Copper	-	52	-	$Cu \rightarrow Cu^{+} + e^{-}$
Copper	-	103	-	$Cu \rightarrow Cu^{++} + 2e^{-}$
Nickel	90	72	78	$Ni \rightarrow Ni^{++} + 2e^{-}$
Carbon steel	74	20	29	$Fe \rightarrow Fe^{++} + 2e^{-}$
Carbon steel	110	29	43	$Fe \rightarrow Fe^{+++} + 3e^{-}$

The accuracy of this method depends on the precision with which the surface profiles can be measured (about 20 percent). Therefore, the efficiencies calculated on the basis of volume of metal removed should not be considered to be as accurate as those determined by traditional weight loss methods. Nevertheless, the current efficiencies of less than 100 percent and the qualitative visual observations of evolved gas support the argument that oxygen was produced during high current density anodic dissolution. The current efficiencies also agree with the observation that greater volumes of gas were evolved during dissolution in nitrate and chlorate solutions than in chloride solutions.

In the case of copper dissolution, small volumes of gas were observed in stagnant solutions, agreeing with Kinoshita's observations.

However, at high current densities and in forced convection, assuming a valence of 2 resulted in a current efficiency of 100 percent. Since gas was observed, the current efficiency must have been less than 100 percent and the apparent valence less than 2. Assuming an apparent valence of 1.6 (which Kinoshita found assuming no oxygen evolution) a current efficiency of 83 percent was computed.

While there is a considerable degree of uncertainty in the calculations, and there are some differences in the results from the several studies cited, three qualitative conclusions can be made: (1) gas was observed, especially in all the high current density experiments, (2) the volume of gas (which was not measured) appeared to vary greatly with different metal/electrolyte combinations, and (3) the evolved gas was probably oxygen, although it may have contained a substantial percentage of water vapor.

E. Periodicities

Kinoshita has shown that copper dissolves into chlorate solutions at high current densities with periodic oscillations of the anode potential.[14] Therefore, an attempt was made to see if this behavior was particular to copper or chlorate solutions.

It is possible that periodic oscillations are the rule rather than the exception during high current density dissolution, but the area over which the oscillations occur is very small. The anodic behavior of copper in chlorate solutions may be the result of a synchronization of these oscillations so they occur in phase over a large surface area. The absence of oscillations in other metals would be explained by oscillations with phases that were randomly distributed,

and would therefore, normally cancel out.

The periodicities observed for copper dissolving into chlorate solutions have been tabulated in Section IV.A.2. Copper, forced convection. These oscillations were very regular in both the observed phenomena (the layers of solid reaction products were of uniform size) and in the electrical phenomena (during one experiment the oscillations were of constant amplitude and period). The amplitude and period of the oscillations were a function of current density and electrolyte flow rate. Since the phenomena observed here differed very little from those previously reported, and mentioned in the results, no further mention of it will be made here.[33]

As mentioned in Section B. Voltage phenomena, many systems showed voltage fluctuations. These fluctuations were never periodic, as with the dissolution of copper into chlorate solutions, where oscillations correlated closely with the formation of solid layers. The fluctuations considered here appeared to be directly related to gas evolution. The layer of gas on the electrode surface probably partially insulated the surface and caused fluctuations in the cell voltage as bubbles were swept off the surface.

As previously mentioned, the dissolution of carbon steel and nickel at 20 amperes/cm^2 was accompanied by large volumes of evolved gas, especially in chlorate solutions. The anode was completely covered with gas, resulting in an increase in the cell voltage great enough to exceed the limits of the present power supply. Therefore, these dissolution experiments were actually conducted at constant voltages and variable current densities. For carbon steel dissolving into chlorate, the periodic shedding of gas from the anode correlated

closely with measured periodic current density oscillations. The amplitude of these oscillations was 20 amperes/cm^2 (from a low of 5 amperes/cm^2 to a peak of 25 amperes/cm^2) and the period of the oscillations was 0.1 seconds/cycle (during a 5 second experiment 53 cycles were recorded). The anodic behavior of nickel was similar, except that the oscillations were not as regular. Jacquot has measured periodic voltage oscillations and an active/transpassive voltage transition from the dissolution of carbon steel into chlorate solutions.[52]

With the dissolution of MONEL K-500 into chlorate solutions and nickel into chloride solutions, at high current densities, solid reaction products were periodically swept off the anode surface. The solids did not form a cohesive layer and there were no voltage fluctuations that correlated with the shedding. This dissolution behavior was similar to that of copper at high current densities. However, as noted in the results, copper did not dissolve at high current densities with its characteristic periodic oscillations. Therefore, the possibility exists that MONEL and nickel would also dissolve with periodic oscillations under some lower current density conditions, but such behavior was not observed here.

VI. CONCLUSIONS

The conclusions of this investigation are outlined below, with the questions that initiated the study.

A. What was the relationship between the phenomena observed visually during anodic dissolution and measured cell voltages?

1. For copper, the completion of an "iris" of solid reaction products was accompanied by a sudden increase in the overall cell voltage.
2. For the remaining metals (except the dissolution of MONEL K-500 into chlorate solutions), no voltage transitions were observed, although irises continued to appear. These irises were much less pronounced than with copper.
3. The active/transpassive transition was not accurately predicted by the criteria of mass transfer limitation of reaction products from the anode into the bulk solution.

B. How general was the formation of solid and gaseous reaction products?

1. Dissolution of copper resulted in the formation of solids under practically all conditions. In stagnant solutions there was also evidence of "jetting" of solid and gaseous products into the bulk solution.
2. The remaining metals generally dissolved with the formation of solid reaction products. However, evolved gas and the occurrence of transparent, highly colored solutions (concentrated salt solutions), sometimes rendered a conclusion as to the presence of solids uncertain.

3. Evolution of gas, probably oxygen, was common and was particularly great with the dissolution of nickel and carbon steel. The presence of substantial amounts of water vapor in the evolved gas was not ruled out.
4. "Pores" were observed in the oxide layer covering copper, after dissolution into nitrate solutions, over a wide range of current densities.
5. Dissolution resulted in surface finishes that depended upon the current density and electrolyte. The observed surface finishes were: "corroded", etched, pitted, and sometimes smooth.

C. Were periodicities found for systems other than copper/chlorate?

1. Copper dissolution into chlorate solutions showed periodic oscillations under a wide range of conditions. However, at high current densities (20 amperes/cm^2) there were no oscillations. No other metal or electrolyte revealed oscillations similar to this.
2. Cell voltage fluctuations, which were distinctly different from the periodic oscillations of copper in chlorate, were observed. These appeared to be caused by anodically evolved gas insulating the electrode surface.

APPENDIX A

The Electrical System

In section II.C. The electrical system, a short description of the electrical components of the apparatus was given. In this appendix additional details and circuit diagrams are provided.

Due to the high filming speeds used, it was necessary to operate the camera, solenoid valve (electrolyte flow), lights, and power source rapidly and easily in a prearranged sequence. Four switches, mounted on one control box actuated all the components. These switches are indicated in the block diagram (Fig. A-1) with the circuits they control.

Switch 1 controlled the lights: two 500-watt photoflood lamps used to illuminate the pen recorder and the fiber optics lamp used to illuminate the anode. Switch 2 controlled a manual relay in series with the electrolysis cell and power supply. Switch 3 actuated the clock (time interval meter), solenoid (electrolyte flow), and a circuit with the camera and timed relay in series. Normally switch 4 (a remote starter for the timed relay) was closed.

In an experiment the switches were closed in the following sequence: switch 1 (which turned on the lights), switch 2, and switch 3 (which started the clock, camera, electrolyte flow, and the timed relay). After a preset time, the timed relay completed the circuit comprised of the power source, electrolysis cell and manual relay. The dissolution experiment began. Switch 2 could be actuated at any time to interrupt the dissolution event, while the camera continued to photograph the anode and the electrolyte continued to flow.

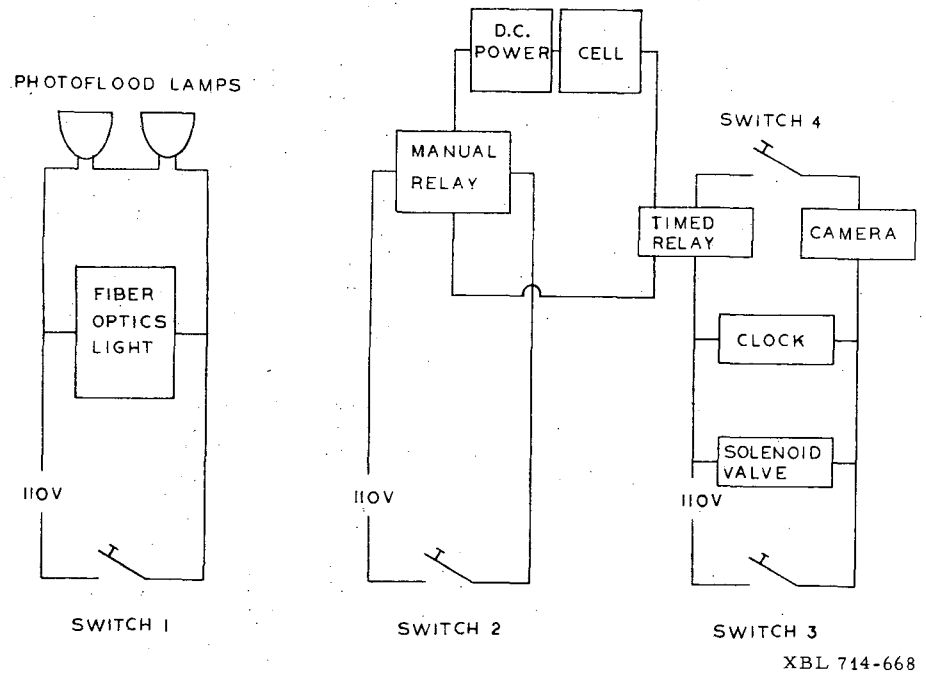

Fig. A-1. Block diagram of the principle circuits in the experimental apparatus.

The wiring diagram, Fig. A-2, shows in more detail how the two relays were connected. With the timed relay in the NC position and the manual relay in the NO position, the two relays were in parallel and the cell was excluded from any complete circuit. The current flowed through the shunt, timed relay and power sink. A small amount of current flowed through the parallel circuit comprised of the manual relay and a d.c. microammeter. The ammeter measured this 'leaking current'. Switching the manual relay to the NC position (by opening switch 2) placed the cell in a circuit parallel with the power supply. Assuming that the cell resistance was comparable to that of the meter, the current which passed through the cell was given by the meter before opening switch 2. This 'leaking current' was on the order of 0.0001 percent of the total current. Very shortly after switch 2 was opened, switch 3 was closed and the timed relay changed to the NO position. At this point the cell was in series with the power supply and all the current passed through the cell. Finally, the manual relay was activated and returned to the NO position. This opened the circuit and ended the electrolysis event. The camera continued to operate and the electrolyte continued to flow until switch 3 was opened.

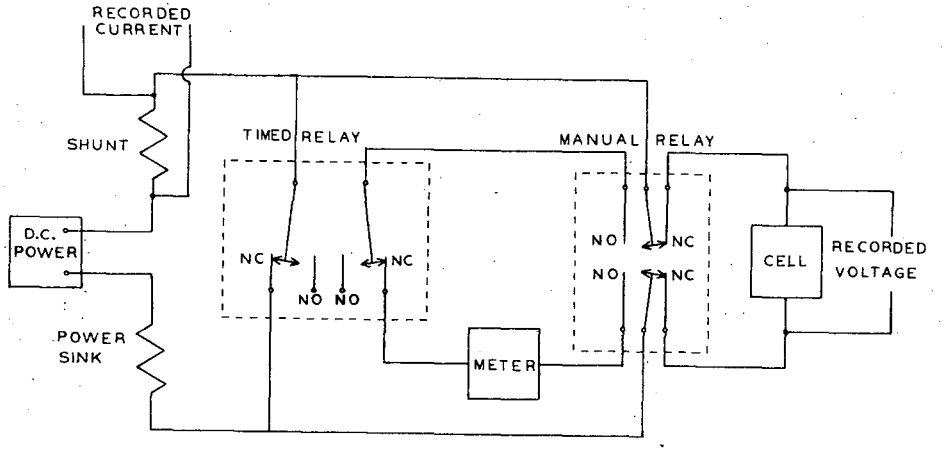

Fig. A-2. Wiring diagram indicating the relationship between the manual relay and the timed relay.

APPENDIX B.

Hydrodynamic Parameters of the Several Flow Systems Used in this Laboratory

Previous experimenters in this laboratory have used three flow channels, each with different dimensions, to study various phenomena at high current densities.[14-20,33,52] A comparison of results among the several studies must take into account the hydrodynamic conditions. Although the flow conditions are often specified in terms of the linear flow velocity, comparisons based on the Reynolds number are often more meaningful. This appendix provides data for both flow channel hydraulic dimensions and electrolyte properties, enabling one to compute Reynolds numbers for the previously reported investigations.

Flow channel hydraulic dimensions

Channel cross section (gap × width)	Hydraulic diameter[a]	Anode dimensions	Reynolds number[b]	References
1mm × 3mm	1.50mm	3mm × 3mm	15u	Kinoshita[14-16,33]
0.521mm × 7.94mm	0.978mm	0.53mm × 3.17mm	10u	Landolt[17-20,52]
6mm × 10mm	7.5mm	5mm × 5mm	75u	This paper

a. hydraulic diameter = 4 (cross sectional area)/perimeter

b. $Re = uD_h/\nu$, where u = linear flow velocity, cm/sec

D_h = hydraulic diameter, cm

ν = kinematic viscosity, cm^2/sec

viscosity/density

The column gives the Reynolds number in terms of the linear flow velocity, assuming $\nu = 10^{-2}$ cm^2/sec.

The kinematic viscosity is often assumed to be 10^{-2} cm^2/sec; the approximate value for water at 20°C. The following table shows that this assumption is in substantial error for concentrated salt solutions.

Experimental[a] kinematic viscosities for 5N solutions, 25°C.

Electrolyte	Kinematic viscosity $\nu \times 10^2$ cm^2/sec
NaCl	1.416
$NaNO_3$	1.286
$NaClO_3$	1.403

a. measured using an Ostwald viscometer; these experimental kinematic viscosities were used to compute the absolute viscosities in Table III.

Literature values for several physical properties are presented in Table B-1 for some electrolytes used by the investigators mentioned above. Physical properties of the electrolytes used in this study are listed in Table III.

Table B-I. Physical properties of some solutions, 25°C

Electrolyte	Concentration	Density g/cm^3	Viscosity centipoise	Kinematic viscosity[k] $\nu \times 10^2$ cm^2/sec	Conductivity[l] 1/ohm-cm
KCl	2N	1.087[a]	0.898[f]	0.826	92.3
KNO_3	2N	1.184[b]	0.898[g]	0.758	69.0
K_2SO_4	1N	1.064[c]	0.998[h]	0.938	71.5
$NaClO_3$	2N	1.135[d]	1.089[i]	0.959	51.7
H_2O	-	0.997044[e]	0.8949[j]	0.8976	-

References for Table B-I

a. Chapman and Newman, p. 126 cites: Jones and Ray. J.A.C.S., 59, 187 (1937) see ref. 30

b. Computed from data in International Critical Tables and Handbook of Chem. and Phys.

c. Chapman and Newman, p. 171 cites: Jones and Ray. J.A.C.S., 59, 187 (1937)

d. Computed from data in International Critical Tables; data for 18°C

e. Handbook of Chemistry and Physics

f. Computed from data in Chapman and Newman, p. 128 cites: Kume and Tanaka. Nippon Kagaku Zasshi, 81, 534 (1960)

g. Computed from data in Chapman and Newman, p. 164-5 cites: Suryanarayana and Venkatesan. Acta Chim. Acad. Sci. Hung., 17, 327 (1958) and International Critical Tables

h. Computed from data in Chapman and Newman, p. 172 cites: Jones and Colvin. J.A.C.S., 62, 338 (1940)

i. Computed from data in International Critical Tables

j. International Critical Tables

k. Computed from density and viscosity data

l. Chemical Engineers' Handbook, 3rd edition, John H. Perry, editor.

APPENDIX C.

A list of Anodic Dissolution Events Filmed

The primary experimental data was in the form of color motion picture film amounting to 3,100 feet (3 rolls of 400 feet each and 19 rolls of 100 feet each). This film has been edited, to add titles and remove poorly exposed film, into eight reels each containing about 400 feet of film. The original film has been deposited in the archives of the Lawrence Berkeley Laboratory. (The film is deposited under the title of "Cinematic Studies--- Hellyar," filing unit code 10***33, shelf location 132-F. Access to this film is restricted.)

The following tables indicate, by reel number, the systems filmed and some of the experimental conditions.

Table C-1. A tabulation of anodic dissolution events filmed.

Reel	Metal	Electrolyte	Current density ampere/cm^2	Flow conditions cm/sec	Filming speed frames/sec	Notes
1	copper	2N $NaClO_3$	3.15	stagnant	32	Voltage trace on oscilloscope, Ektachrome ECO film, front and side views. Electrode 1/8" diameter
	"	"	11	"	"	
	"	"	3.2	"	"	
	"	2N $NaClO_3$	3.15	"	"	Ektachrome EFB, front and side views, oscilloscope recorded voltage trace
	"	2N KNO_3	"	"	"	
	"	2N KCl	"	"	"	
	"	1N K_2SO_4	"	"	"	
	"	2N $NaClO_3$	"	"	64	1/8" diameter electrode
	"	2N $NaClO_3$	"	"	32	Voltage trace on paper pen recorder. OFHC copper
2	copper	2N $NaClO_3$	4	40	32	Two events, 40 feet of each.
	"	"	4	25	32	One electrode repeatedly dissolved.

Table C-1, continued

Reel	Metal	Electrolyte	Current density ampere/cm^2	Flow conditions cm/sec	Filming speed frames/sec	Notes
	HASTELLOY X	2N KNO_3	1,4,8, 20, and 40	150	32	
3	copper	5N NaCl	1 & 20	10	64	All the experiments on Reels 3 and 4 were done on the same format.
	nickel	"	"	"	"	
	carbon steel	"	"	"	"	Full title on these reels
	MONEL K-500	"	"	"	"	
	INCONEL X-750	"	"	"	"	
	HASTELLOY X	"	"	"	"	
	copper	5N $NaNO_3$	"	"	"	
	nickel	"	"	"	"	
	carbon steel	"	"	"	"	
4	MONEL K-500	5N $NaNO_3$	1 & 20	10	64	

Table C-1, continued

Reel	Metal	Electrolyte	Current density ampere/cm^2	Flow conditions cm/sec	Filming speed frames/sec	Notes
	INCONEL X-750	5N $NaNO_3$	1 & 20	10	64	
	HASTELLOY X	"	"	"	"	
4	copper	5N $NaClO_3$	"	"	"	
	MONEL K-500	"	"	"	"	
	INCONEL X-750	"	"	"	"	
	HASTELLOY X	"	"	"	"	
5	copper	2N KNO_3	40	150	1,000	HYCAM About 175 feet of good film.
6	copper	2N KNO_3	40	150	4,000	HYCAM, special processing, about 300 feet of film
7	copper	2N KNO_3	40	150	4,000	HYCAM, special processing, full 400 feet of film

Table C-1, continued

Reel	Metal	Electrolyte	Current density ampere/cm^2	Flow conditions cm/sec	Filming speed frames/sec	Notes
8	copper	1N K_2SO_4	3.15	stagnant	12 to 64	Exposure tests
	"	2N $NaClO_3$	3.15	"	32	Exposure tests
	"	2N $NaClO_3$	3.15	"	32	Overexposed films showing the entire cell overexposed
	"	2N KCl	1.6	"	32	
	"	2N $NaClO_3$	4	40	1,000	HYCAM, black-and-white exposure test

ACKNOWLEDGEMENT

"We are made to exaggerate the importance of that work we do; and yet how much is not done by us!"

Henry David Thoreau

This work was done under the auspices of the United States Atomic Energy Commission.

REFERENCES

1. Electrochemical Machining, edited by A. E. DeBarr and D. A. Oliver (American Elsevier Publishing Company, Inc., 1968).
2. John F. Kahles, Electrochemical Machining (ECM), Metals Handbook, 3, 233-40 (1970).
3. A. H. Meleka, Electrochemical Machining, Science Journal, 3, 50-5 (1967).
4. H. Tipton, The Dynamics of Electrochemical Machining, Proc. of the 5th Int'l. Machine Tool Design Research Conference, University of Birmingham (1964). [published in: Advances in Machine Tool Design and Research, edited by S. A. Tobias and F. Koenigsberger, Pergamon Press, Oxford, 509-22 (1965).]
5. J. Hopenfeld and R. R. Cole, Prediction of the One-Dimensional Equilibrium Cutting Gap in Electrochemical Machining, J. Eng. for Industry (Trans. ASME), 91, 755-65 (1969).
6. J. Hopenfeld and R. R. Cole, Electrochemical Machining-Prediction and Correlation of Process Variables, J. Eng. for Industry (Trans. ASME), 88, 455-61 (1966).
7. J. W. Cuthbertson and T. S. Turner, Electrochemical Machining-a study of the effects of some variables, The Production Engineer (London), 45, 270-81 (1966).
8. J. W. Cuthbertson and T. S. Turner, Electrochemical Machining-some further studies of process variables, The Production Engineer (London), 46, 24-31 (1967).
9. G. L. Baldwin, D. C. Brown, and J. L. Gulati, Electrochemical Machining-Nomograms for Prediction of Process Parameters. The Engineer (London), 225, 307.12(1968).

10. James P. Hoare, Michell A. Laboda, Michael L. McMillan, and Augustine J. Wallace, An Investigation of the Difference Between NaCl and $NaClO_3$ as Electrolytes in Electrochemical Machining, J. Electrochem. Soc., 116, 199-203 (1969).

11. A. D. Davydov, V. D. Kashcheev, and B. N. Kabanov, Anodic Solution of Metals at High Current Densities, Elektrokhimiya, 5, 221-5 (1969).

12. DerTau Chin, Anodic Mechanism of Electrochemical Machining: Study of Current Transient on a Rotating Electrode, J. Electrochem. Soc., 118, 174-9 (1971).

13. P. J. Boden and P. A. Brook, Electrochemical Principles of ECM, The Production Engineer (London), 48, 408-17 (1969).

14. Kimio Kinoshita, Studies on the Anodic Dissolution of Copper at High Current Densities, Ph. D. Thesis, University of California, Berkeley (1969). [published as: UCRL-19051]

15. K. Kinoshita, D. Landolt, R. H. Muller, and C. W. Tobias, Stoichiometry of Anodic Copper Dissolution at High Current Densities, J. Electrochem. Soc., 117, 1246-51 (1970).

16. K. Kinoshita, R. H. Muller, and C. W. Tobias, Oxygen Evolution in High-Rate Anodic Metal Dissolution, UCRL-20339, December 1970.

17. D. Landolt, R. H. Muller, and C. W. Tobias, High-Rate Anodic Dissolution of Copper, J. Electrochem. Soc., 116, 1384-90 (1969).

18. D. Landolt, R. H. Muller, and C. W. Tobias, Anode Potentials in High-Rate Dissolution of Copper, J. Electrochem. Soc., 118, 40-5 (1971).

19. D. Landolt, R. H. Muller, and C. W. Tobias, Crystallographic Factors in High-Rate Anodic Dissolution of Copper, J. Electrochem. Soc., 118, 36-40 (1971).

20. D. Landolt, R. Acosta, R. H. Muller, and C. W. Tobias, An Optical Study of Cathodic Hydrogen Evolution in High-Rate Electrolysis, J. Electrochem. Soc., 117, 840-45 (1970).

21. "Kodak Ektachrome Films for Photo Instrumentation, Photographic and Physical Properties," Kodak pamphlet P-42, Eastman Kodak Company, Rochester, N.Y. 14650.

22. "Hycam High-Speed Motion Picture Cameras," Red Lake Laboratories, Inc., Santa Clara, Ca. 95051.

23. "Huntington Nickel Alloys," Huntington Alloy Products Division, The International Nickel Company, Inc., New York.

24. Michell A. Laboda and Michael L. McMillan, A New Electrolyte for Electrochemical Machining, I. Development Studies, Electrochem. Technology, 5, 340-6 (1967).

25. "Composition of Standard Steels," Metals Handbook, 3, 62 (1970).

26. "MONEL Nickel-Copper Alloys," The International Nickel Company, Inc., New York.

27. "Engineering Properties of INCONEL X-750" (Technical Bulletin T-38), The International Nickel Company, Inc., New York.

28. "HASTELLOY alloy X," Stellite Division, Cabot Corporation, Kokomo, Indiana.

29. D. T. Chin and A. J. Wallace, Jr., Electrochemical Machining: A Note on the Throwing Power of Electrolytes, J. Electrochem. Soc., 118, 831-33 (1971).

30. Thomas W. Chapman and John Newman, A Compilation of Selected Thermodynamic and Transport Properties of Binary Electrolytes in Aqueous Solution, UCRL-17767, May 1968.

31. Lange's Handbook of Chemistry, 10th edition, (The McGraw-Hill Book Company, New York) p. 1021 (1961).

32. Handbook of Chemistry and Physics, 47th edition, (The Chemical Rubber Company, Cleveland, Ohio) B-191 (1966).

33. J. Cooper, R. H. Muller, and C. W. Tobias, Periodic Phenomena in Copper Dissolution at Constant Current, Fundamentals of Electrochemical Machining, edited by Charles L. Faust, (The Electrochemical Society, Princeton, New Jersey) 300-15 (1971).

34. J. M. Evans and P. J. Boden, Surface Finish Produced During Electrochemical Machining on Nickel and Nimonic 80A in Chloride Electrolytes, Fundamentals of Electrochemical Machining, edited by Charles L. Faust, (The Electrochemical Society, Princeton, New Jersey) 40-62 (1971).

35. William G. Moffatt, George W. Pearsall, and John Wulff, The Structure and Properties of Materials, Vol. I Structure, (John Wiley & Sons, Inc., New York) 92, 129 (1964).

36. F. S. Bromfeld, The Hydrodynamic Entry Length in Rectangular Channels, Ph. D. Thesis, University of Washington, 30 (1964).

37. R. Bird, W. E. Stewart, and E. N. Lightfoot, Transport Phenomena, (John Wiley, New York) 47 (1960).

38. John Newman, Engineering Design of Electrochemical Systems, Ind. Eng. Chem., 60(4), 12-27 (1968).

39. P. VanShaw, L. P. Reiss, and T. J. Hanratty, Rates of Turbulent Transfer to a Pipe Wall in the Mass Transfer Entry Region, A.IICH.E. Journal, 9, 362-4 (1963).

40. T. P. Hoar, The Anodic Behavior of Metals, Modern Aspects of Electrochemistry, edited by J. O'M. Bockris (Academic Press, New York) 2, 262-342 (1959).

41. A. Pigeaud and H. B. Kirkpatrick, A Correlated Potentiostatic Microscopic Study of Iron Passivation in Sulfuric Acid, Corrosion, 25, 209-14 (1969).

42. J. Friedel, Annealing, Polygonization, Recrystallization, Grain Boundaries (Chapter X), Dislocations, (Pergamon Press, Oxford) 275-302 (1964).

43. S. Amelinckx, Surface Methods (Chapter 1), The Direct Observation of Dislocations, Supplement 6 to Solid State Physics, Advances in Research and Applications, (Academic Press, New York) 1-53 (1964).

44. F. W. Young and N. Cabrera, Partial Polygonization in Impure Copper Crystals, J. Appl. Phys., 28(7), 787-91 (1957).

45. F. W. Young, Etch Pits at Dislocations in Coper, J. Appl. Phys., 32(2), 192-201 (1961).

46. L. C. Lovell and J. H. Wernick, Dislocation Etch Pits and Polygonization in High-Purity Copper, J. Appl. Phys., 30(4), 590-2 (1959).

47. E. Votava, Electron Microscopic Investigation of the Polygonization and Recrystallization of High Purity Copper, Acta Metallurgica, 9,870-9 (1961).

48. Vola Price Barton, Light Sensitivity of Cuprous Oxide and of Selenium, Phys. Rev., 23 (Series 1), 337-44 (1924).

49. Allen D. Garrison, The Behavior of Cuprous Oxide Photo-voltaic cells, J. Phys. Chem., 27, 601-22 (1923).

50. T. N. Grechukhina and A. Sh. Valeev, Study of the Mechanism of the Anodic Dissolution of Copper In Phosphoric Acid, II. Photoelectrochemical Effects, Elektrokhimiya, 3, 1080-5 (1967).

51. Jerome Kruger and Joan P. Calvert, The Oxide Films Formed on Copper Single Crystal Surfaces in Water, III. Effect of Light, J. Electrochem. Soc., 111, 1038-41 (1964).

52. Daniel Jacquot, unpublished results

53. Donald J. Royer, Jacob Kleinberg and Arthur W. Davidson, The Anodic Behavior of Copper in Aqueous Solutions, J. Inorg. Nucl. Chem., 4, 115-27 (1957).

TECHNICAL INFORMATION DIVISION
LAWRENCE BERKELEY LABORATORY
UNIVERSITY OF CALIFORNIA
BERKELEY, CALIFORNIA 94720